Journal of Thermal Science Vol.32, No.5 (2023) 1912−1934

https://doi.org/10.1007/s11630-023-1848-1 **Article ID: 1003-2169(2023)05-1912-23**

Experimental Study on Product Characteristics of Typical Pulverized Coal Preheated by a Self-Preheating Burner

ZHANG Jinyang[1,2], OUYANG Ziqu[1,2,3*], DING Hongliang[2,3], SU Kun[2,3]

1. Research Center of Fluid Machinery Engineering and Technology, Jiangsu University, Zhenjiang 212013, China
2. Institute of Engineering Thermophysics, Chinese Academy of Sciences, Beijing 100190, China
3. University of Chinese Academy of Sciences, Beijing 100049, China

Abstract: As the major primary energy source in China, coal has been proved to be capable to improve its physical and chemical characteristics by the pretreatment of the self-preheating burner. In this study, the effects of altering operating conditions including preheating temperature (T_p) and primary air equivalence ratio (λ_p) on preheating characteristics of three typical pulverized coal were investigated on a bench-scale test rig. The high-temperature coal gas compositions along the axis of the riser and at the outlet of the self-preheating burner were measured, and the coal char and coal tar produced in the preheating process were collected and analyzed separately. The results indicated that with the significant release of volatile and the occurrence of chemical reactions, cracks and micropores emerged on the surface of the particles, making the pore structure on the surface more developed, and T_p had the most significant effect on the structure of coal particles. Additionally, there were evident differences in the corresponding operating conditions when the preheating characteristics of the three typical coal reached optimally. And preheating had the strongest influence on the degree of anthracite modification. With respect to coal tar, the increase of T_p and λ_p further promoted its secondary cracking and oxidation, resulting in a decrease in production yield. In this study, for bituminous coal and lignite, a large amount of coal tar were produced during preheating and the highest production yields could reach 5.74% and 6.15%, respectively. While for anthracite, the production yield was intensely low due to its own coal properties, all below 1.02%.

Keywords: self-preheating, fuel modification, product characteristics, coal particle structure, coal tar

1. Introduction

Energy is an essential physical condition for humanity survival and social production and development. In present-day society, coal, as one of the three energy pillars coexisting with oil and natural gas in today's world economy is playing an indispensable role in promoting the operation and development of the entire world economy [1–3]. Coal is the most important primary energy source in China, accounting for 56% in 2021 [4], and its reserves accounted for 94.22% of the total primary energy [5]. For a considerable period of time in the future, raw coal consumption will remain an important part of energy consumption in China [6].

Received: Nov 22, 2022
GE: DUAN Lunbo
Corresponding author: OUYANG Ziqu E-mail: ouyangziqu@iet.cn

Currently, global climate change has become a severe issue to be jointly tackled by humans. The greenhouse gases produced and emitted by the human race in daily life and production are considered to be the main cause of global warming and have received much attention [7]. Among them, fossil fuel consumption is the core of common concern to human society [8], and thus coal is certainly included.

As the largest developing country and the largest CO_2 emitter in the world, China has taken addressing climate change as a major strategy for economic and social development. Additionally, carbon emission reduction in coal and relevant industries performs a decisive function in achieving the national goal of "carbon neutrality" [9]. In order to address issues related to coal-based carbon emission reduction and achieve the efficient, clean and low-carbon utilization of coal, new requirements have been made for scientific and technological innovation in the field of engineering thermophysics. In particular, traditional coal-fired industry has ushered in new challenges.

Inspired by high-temperature air combustion technology, the Institute of Engineering Thermophysics, Chinese Academy of Sciences (IET, CAS) proposed a high-temperature combustion method [10] of pulverized coal suitable for high-efficiency and low nitrogen combustion of solid fuels, and based on this, developed the coal self-preheating combustion technology that made use of the advantages of circulating fluidized bed such as wide fuel adaptability, good combustion stability, low NO_x emission and no external heat source required. Going through significant physical and chemical changes in the preheating process, the fuel could be modified, activated and denitrified, and subsequently the air-staged combustion technology was combined to further reduce NO_x and increase the combustion efficiency in the combustion process.

Some scholars have explored the preheating characteristics of pulverized coal applying coal self-preheating combustion technology. Wang [11] found that the particle size of Yangquan anthracite was significantly reduced after preheating in a circulating fluidized bed, and the median particle size (d_{50}) decreased from 82 μm to 19 μm. Additionally, the specific surface area and the total pore volume both increased significantly, which was beneficial to the diffusion of oxygen on the solid surface of the preheated fuel, thus enhancing the combustion effect. Ouyang [12, 13] carried out a series of experiments on a bench-scale rig, finding that preheated anthracite could be obtained steadily and continuously at a low air equivalence ratio, and d_{50} of preheated anthracite decreased while the specific surface area increased, which was consistent with Wang' research [11]. Furthermore, the effect of preheating temperature (T_p) on particle characteristics was investigated. For preheated fuel, the specific surface area and pore volume mainly depended on the pores in microsize with a diameter less than 2 nm and meso-size with diameters between 2–10 nm. When T_p<900°C, the specific surface area and pore volume increased with the increase of T_p, while when T_p>900°C, they were inversely proportional to T_p. After preheating, a large number of cracks and pores appeared on the particle surface, and the pore structure was well developed. In Zhu's studies [14, 15], during the preheating, the surface of coarse particles was obviously broken and fine particles attached to the surface, so the contact area between oxygen and coarse particles decreased. Although the contact area was lessened, the high-calorific gas generated in the process played a very important role in the subsequent stable combustion. Zhu also found that 41.4% of fuel-bound nitrogen converted to N_2 in the self-preheating burner, creating conditions for reducing NO_x emissions. In Zhang's research [16–18], it was found that the graphitization degree of carbon frame structure would decrease during the preheating process, and stable carbon frame structure was transformed into a disordered active defect structure, thus enhancing the combustion reactivity. In addition, Zhang also summarized some merits of preheated char, such as smaller particles, larger surface area, more developed pore structure, and better combustion activity compared with raw coal. Researchers Ding, Zhang and Su also explored the factors affecting preheating characteristics. Ding's research [19] found that when d_{50}=163.84 μm, the particle size range of Shenmu semi-coke decreased most significantly and had better activity to help the subsequent combustion process. Meanwhile, the smaller the particle size of Shenmu semi-coke, the smaller the difference between before and after particle preheating modification. Zhang's discoveries [20] were that an increase of BET surface area, an expansion of pore structure, an increase of light aromatic rings, and a decrease of graphitization degree in gasified char as influencing factors all enhanced gasification reactivity. Su [21] found that the preheating fuel jet velocity had a significant effect on the preheating characteristics. With the increase of preheating fuel jet velocity from 7.41 m/s to 15.17 m/s, the transformation of all components in gas except CO_2 increased first and then decreased, while CO_2 showed an opposite trend. Moreover, the particle size of coal coke decreased first and then increased, and the specific surface area and reactivity increased first and then decreased. Therefore, there can be an optimum preheating fuel jet velocity to obtain the optimum preheating characteristics.

The above research results showed that some progress has been made in the analysis of preheating

characteristics of a variety of coal types. By summarizing the above contents, it could be drew a consistent conclusion that after preheating, the particle size of pulverized coal became smaller, and the specific surface area and total pore volume increased, which was conducive to improve the fuel combustion effect and the reaction activity. Nevertheless, many researchers often chose only one or a few types of coal for targeted research, and did not make a detailed comparison of the preheating characteristics among different types of coal, which limited the broadening of fuel adaptability of the coal self-preheating combustion technology. Additionally, in previous studies, it was difficult to maintain a single change of variables; for example, to study the effect of T_p on fuel preheating characteristics, it was necessary to adjust λ_p or coal feed rate to realize the change of T_p. However, both λ_p and T_p had influence on fuel preheating characteristics, and thus the original research could not accurately analyze the influence of single variable of T_p during preheating process. What's more, the special environment of partial gasification and combustion in the self-preheating burner might also determine that coal tar would release as a product, but previous studies had ignored the production yield of coal tar during preheating. In order to obtain the modification mechanism of different types of coal, the influence of single variable on the fuel preheating characteristics was accurately analyzed, and the preliminary study on coal tar during preheating was complemented. Based on the coal self-preheating combustion technology, the effects of T_p and λ_p on the fuel preheating characteristics of three typical coals during preheating were studied by means of electric heating device temperature control on a 30 kW bench-scale test rig with controllable temperature, in order to accurately analyze the coal conversion characteristics during preheating and support the development and application of the coal self-preheating combustion technology.

2. Experimental

2.1 Test rig

A 30 kW self-preheating combustion test rig for pulverized coal was designed, composed of a self-preheating burner, a down-fired combustor (DFC), and other auxiliary systems, as shown in Fig. 1. The self-preheating burner was designed on the basis of circulating fluidized bed using heat-resistant steel material, composed of a riser with inner diameter 90 mm and height 1500 mm, a cyclone separator, a loop seal and other components. The primary air was supplied from the bottom of the riser, and its volume was about 20%–40% of the theoretical air volume. The fuel entering the self-preheating burner could be quickly ignited and partially burned under the heat storage effect of high-temperature bed material, increasing the temperature to above 800°C. The coal gas and coal char (collectively referred to as preheated fuel) were produced after pulverized coal passed through the self-preheating burner.

The self-preheating burner was equipped with five K-type thermocouples which were placed at the bottom (T1), middle (T2), and top (T3) of the riser, as well as the loop seal (T4) and the outlet of the cyclone separator (T5). Each experimental case carried out in this study ran steadily for about 2 hours. In the sampling process, the temperature fluctuation of each measuring point of the system was controlled by ± 5°C.

Five sampling ports along the axis of the riser were located at 250 mm (SPD-1), 550 mm (SPD-2), 850 mm (SPD-3), 1150 mm (SPD-4), and 1450 mm (SPD-5) from the bottom, respectively. In addition, there was a sampling port at the outlet of the cyclone separator. Water cooling equipment was used to cool the sample temperature throughout the sampling process to ensure that the composition of the sample did not continue to react during the sampling process. The aforementioned

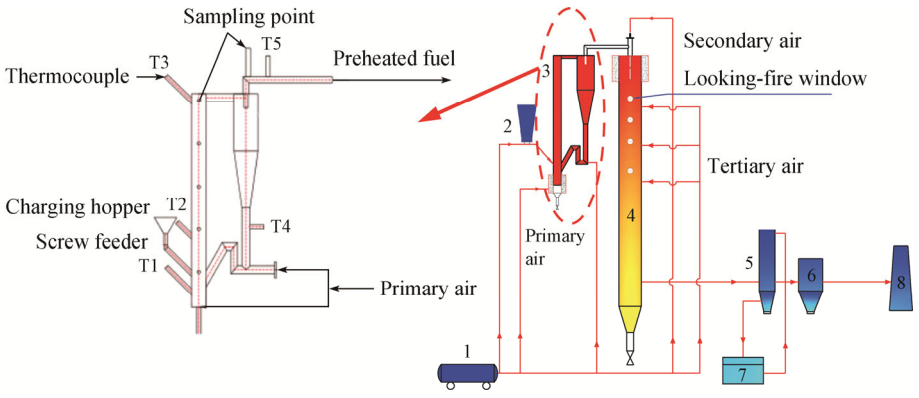

1. Air compressor, 2. Coal feeder, 3. Self-reheating burner, 4. The DFC, 5. Water cooler, 6. Bag filter, 7. Water tank, 8. Chimney

Fig. 1 Schematic diagram of the 30 kW self-preheating combustion text rig

five sampling ports were mainly used to analyze the coal gas composition. The sampling port at the outlet not only obtained coal gas but also collected coal char and coal tar. The solid portion of the cooled preheating product is collected through a cartridge with a filter element. The former was used for particle size analysis, BET analysis, Raman spectrum analysis, and coal properties analysis, while the latter was used for tar quality determination and composition analysis.

2.2 Fuel characteristics

Shenmu bituminous coal (SM coal), Jincheng anthracite (JC coal), and Inner Mongolia lignite (ML coal) were used as experimental fuels in this study. Their properties (ultimate and proximate analysis) are shown in Table 1, and their particle size was controlled at 0–0.18 mm so as to meet the requirements of the actual engineering applications. The particle size distribution of pulverized coal was determined by Mastersizer 2000 laser analyzer, as shown in Fig. 2. The 50% cut size (d_{50}) of SM, JC, and ML was 36.51 μm, 33.82 μm, and 40.77 μm, respectively. Before the experiment, quartz sand was added to the self-preheating burner as heat storage bed material, with a particle size range of 0.1–0.7 mm.

2.3 Experimental conditions

The experimental conditions are listed in Table 2. In this study, all experiment cases strictly adopted the control variable method. The thermal load of the three pulverized coal was controlled to be the same, all of which were 37.87 kW. In the table, λ_p represents the ratio of primary airflow to the theoretical combustion air. T_p represents the highest temperature in the self-preheating burner. In the course of the experiment, an auxiliary heater that can heat silicon rods to raise the temperature was used to control T_p.

T_p and λ_p are two important factors affecting pulverized coal modification, and they often alter simultaneously. In this study, the effects of simultaneous change of T_p and λ_p on the modification of pulverized coal are discussed. Additionally, the purpose of using the auxiliary heater is to accurately control T_p without changing λ_p, so that T_p becomes a single variable affecting the experiment. Furthermore, T_p can be kept constant by adjusting the auxiliary heater, so as to ensure that λ_p is the only variable. For better analysis and discussion, the experimental conditions were grouped, as listed in Table 3. Groups 1–3 intended to explore the comprehensive effects of T_p and λ_p on preheating characteristics of different coal. Groups 4–6 intended to explore the single effects of T_p on preheating characteristics of different coal. Groups 7–9 respectively intended to explore the single effects of λ_p on preheating characteristics of different coal. In group 7, SM coal was taken as the research object to study the effects of changing the λ_p. As for control group, the T_p of Case 2 (λ_p=0.40) and Case 4

Table 1 Ultimate and proximate analysis of the three pulverized coal

Coal type	Ultimate analysis /wt% (air dry)					Proximate analysis/wt% (air dry)				Low heating value
	C	H	O	N	S	M	FC	V	A	Q_{net}/MJ·kg^{-1}
SM coal	72.44	4.06	11.13	1.02	0.55	5.06	56.83	32.37	5.74	28.04
JC coal	70.44	2.36	2.16	0.6	2.81	0.93	71.84	6.53	20.7	25.96
ML coal	71.65	4.56	6.39	0.83	0.52	1.23	43.87	40.08	14.82	28.39

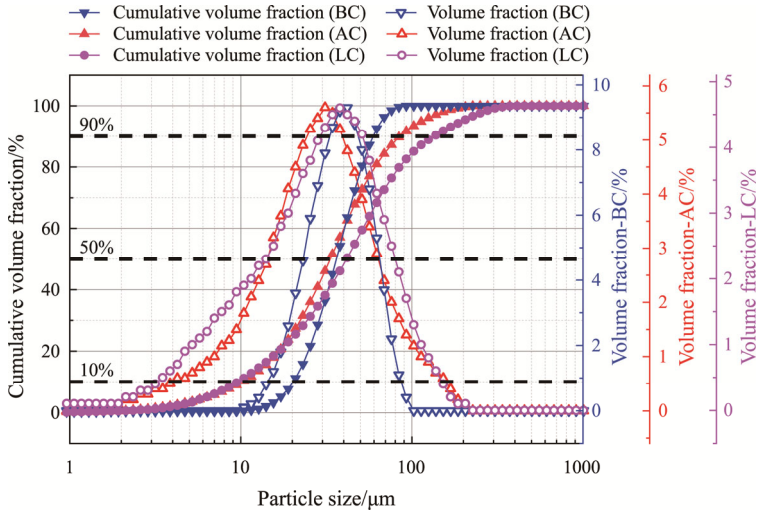

Fig. 2 Particle size distribution curve

Table 2 Experimental conditions

Parameter	Fuel	Particle size/ mm	Fuel feed rate/ kg·h^{-1}	Thermal load/ kW	Preheating temperature/ °C	Auxiliary heater power/ kW	M_P/ m^3·h^{-1}	λ_P/ –
Case 1		0–0.18	4.87	37.87	852	0	12.61	0.36
Case 2		0–0.18	4.87	37.87	901	0	13.96	0.40
Case 3	SM coal	0–0.18	4.87	37.87	954	0	15.69	0.45
Case 4		0–0.18	4.87	37.87	902	0.44	12.61	0.36
Case 5		0–0.18	4.87	37.87	952	1.42	12.61	0.36
Case 6		0–0.18	5.26	37.87	853	0	11.76	0.32
Case 7		0–0.18	5.26	37.87	904	0	12.86	0.35
Case 8	JC coal	0–0.18	5.26	37.87	950	0	14.52	0.40
Case 9		0–0.18	5.26	37.87	903	0.86	11.76	0.32
Case 10		0–0.18	5.26	37.87	949	1.73	11.76	0.32
Case 11		0–0.18	4.78	37.87	852	0	11.64	0.33
Case 12		0–0.18	4.78	37.87	899	0	13.45	0.38
Case 13	ML coal	0–0.18	4.78	37.87	950	0	14.78	0.42
Case 14		0–0.18	4.78	37.87	900	0.36	11.64	0.33
Case 15		0–0.18	4.78	37.87	953	1.21	11.64	0.33

Note: M_p-Primary air flow (m^3/h), λ_P-Primary air ratio

Table 3 Experimental groups

Experimental groups	1	2	3	4	5	6	7	8	9
Experimental condition	Case 1 Case 2 Case 3	Case 6 Case 7 Case 8	Case 11 Case 12 Case 13	Case 1 Case 4 Case 5	Case 6 Case 9 Case 10	Case 11 Case 14 Case 15	Case 2 Case 3 Case 4 Case 5	Case 7 Case 8 Case 9 Case 10	Case 12 Case 13 Case 14 Case 15

(λ_p=0.36) was about 900°C, while that of Case 3 (λ_p=0.45) and Case 5 (λ_p=0.36) was about 950°C. In group 8, JC coal was taken as the research object to study the effects of changing λ_p. As for control group, T_p of Case 7 (λ_p =0.35) and Case 9 (λ_p = 0.32) was about 900°C, while that of Case 8 (λ_p=0.40) and Case 10 (λ_p=0.32) was about 950°C. In group 9, ML coal was taken as the research object to study the effects of changing λ_p. As for control group, the T_p of Case 12 (λ_p=0.38) and Case 14 (λ_p=0.33) was about 900°C, while that of Case 13 (λ_p=0.42) and Case 15 (λ_p=0.33) was about 950°C.

2.4 The running state of the self-preheating burner

Take Case 5 as an example to illustrate the stability of the preheating process of the preheating burner. The temperature fluctuation of each part of the preheating burner is shown in Fig. 3. When the working condition was stable, the highest temperature appeared in the middle of the riser, and its value was 952°C. The temperature in the preheated burner was stable and does not change significantly with time. It showed that the test results of this test are obtained under the normal and stable operation of the self-preheating burner, which was of value and reference significance.

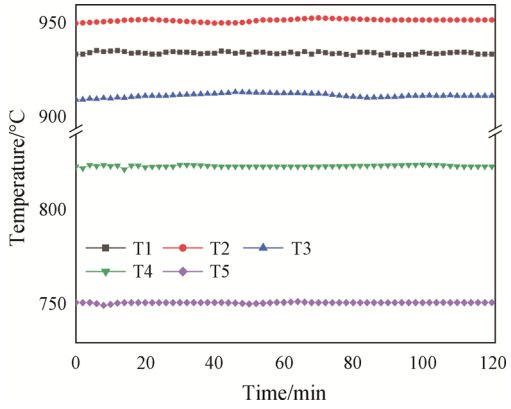

Fig. 3 Temperature distribution curve during preheating process in Case 5

3. Results and Discussion

3.1 Coal char characterization

3.1.1 Comprehensive effects of preheating temperature and primary air equivalent ratio

The specific surface area, total pore volume, and average pore diameter of raw coal and coal char are

shown in Fig. 4. In all operating conditions, T_p was adjusted by changing λ_p, and the corresponding experimental groups were Groups 1–3. In comparison with raw coal, the specific surface area, total pore volume, and average pore diameter of the coal char increased, accompanied by developed pores and improved physical structure, which was consistent with the conclusions of Refs. [22–27]. With the increase of λ_p and T_p, the specific surface area, total pore volume, and average pore diameter of SM coal char all decreased, while the specific surface area of JC coal char and ML coal char increased first and thereafter decreased. Since the particles were subjected to strong thermal stress in the fluidization preheating process, the large particles were gradually broken. Furthermore, with the significant release of volatile and the occurrence of chemical reactions, cracks and micropores were exceedingly likely to emerge on the surface of the particles, making the pore structure on the surface more developed. Additionally, the functional groups and branches of the macromolecular structure were destroyed during preheating, and they formed small molecules that were again attached to the char in the process of migrating to the outward surface [28, 29]. Furthermore, in the self-preheating burner, in addition to the reaction, the secondary crushing caused by the collision between particles and the collision between particles and the wall is also another main reason for the change of particle surface. By comparison, the structure of anthracite coal particles converted more significantly in the preheating process, and their specific surface area greatly increased compared to that of raw coal. It could be judged tentatively that the optimal modification effect of SM emerged at λ_P=0.36, T_p=852°C, while that of JC and ML λ_P=0.35, T_p=904°C and λ_P=0.38, T_p=899°C, respectively.

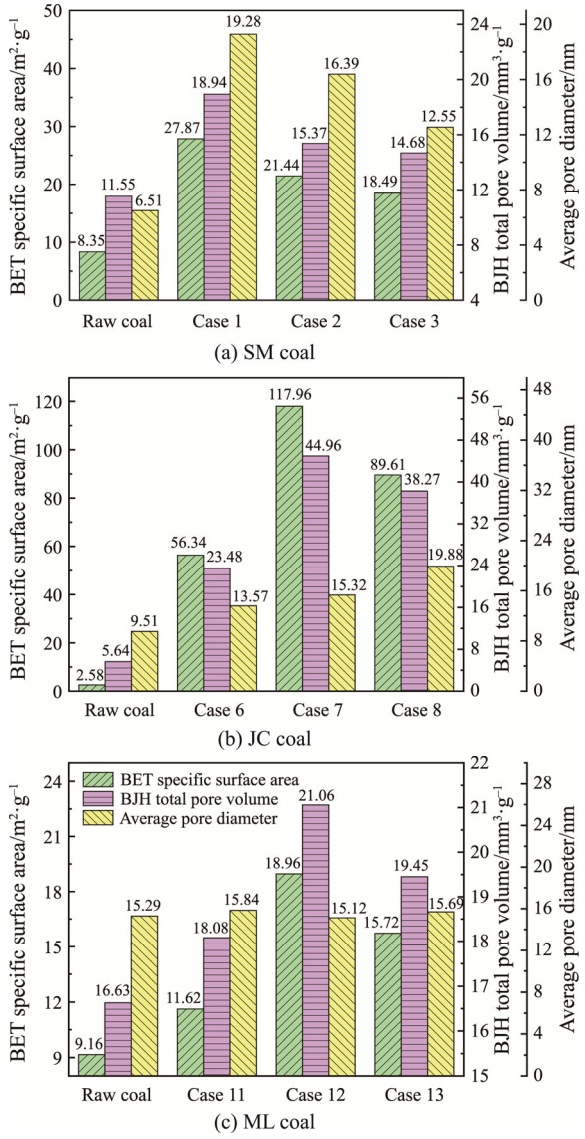

Fig. 4 The specific surface area, total pore volume and average pore size of raw coal and coal char

Raman spectroscopy was mainly utilized to analyze carbon microcrystalline structure. Fig. 5 shows Raman spectra of raw coal and coal char. There was a Gaussian band (1580 cm^{-1}) called G band [30] and four Lorentzian bands (1350 cm^{-1}, 1620 cm^{-1}, 1530 cm^{-1}, 1150 cm^{-1}) called D1, D2, D3 and D4 bands, respectively [31, 32]. The ratios of the areas of different spectral bands represented different meanings [33, 34]. To intuitively analyze the changes in carbon microcrystalline structure, the relative areas of the spectral bands were calculated, as shown in Fig. 6. I_G/I_{All} denoted the graphitization degree, which reflected the degree of perfection of graphite crystal structure; that is, the degree of regularity of the arrangement of carbon atoms in the graphite structure. $(I_{D3}+I_{D4})/I_G$ characterized the active site ratio of carbon framework structures in coal samples, and I_{D1}/I_G reflected the defect density of carbon. In comparison with raw coal, I_G/I_{All} of the coal char showed a downward trend, while I_{D1}/I_G and $(I_{D3}+I_{D4})/I_G$ increased, which was attributed to the depolymerization and devolatilization of raw coal at a higher heating rate. Consequently, the macromolecular carbon chain in the aromatic layer structure was broken, generating small molecular volatile and lowering the graphitization degree in the carbon frame structure [35, 36]. The stable and ordered graphitized structure is transformed into a disordered and highly active defect structure. With the increase of T_P and λ_P, I_G/I_{All} of SM coal char increased while I_{D1}/I_G and $(I_{D3}+I_{D4})/I_G$ decreased, indicating the increase in the graphitization degree but the decrease in the active defect carbon structure, which was consistent with the continuous change in the specific surface area (Fig. 4). In addition, the decrease of specific surface area and total pore volume also demonstrated that the release of volatile would be hindered, and the time required for the

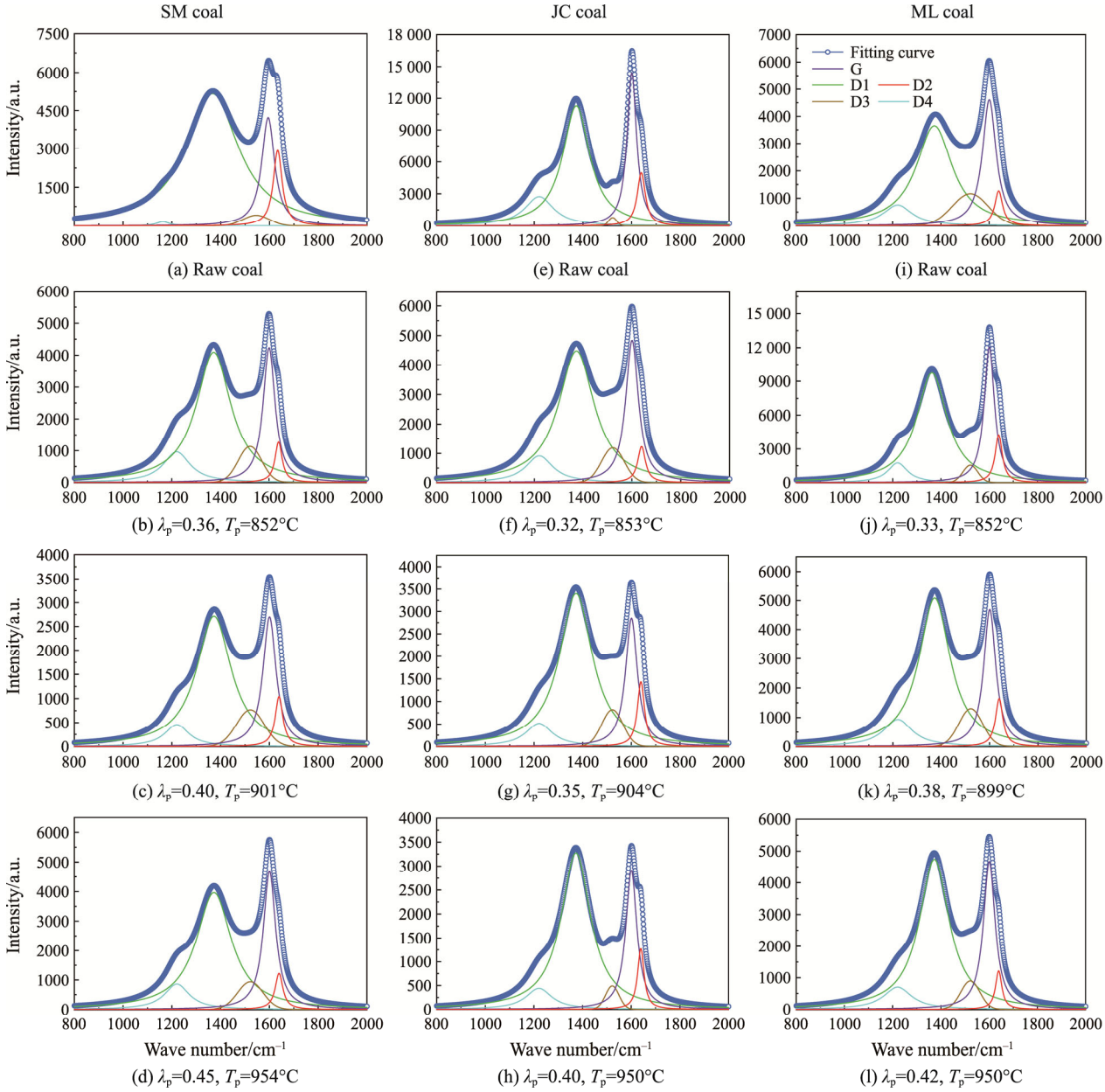

Fig. 5 Raman spectra of raw coal and coal char

temperature difference between internal and external surfaces to reach equilibrium was also prolonged, also suggesting that increasing T_P and λ_P was not conducive to the improvement of SM coal char combustion characteristics. However, with the increase of T_P and λ_P, I_G/I_{All} of JC coal char and ML coal char first decreased and thereafter increased, while I_{D1}/I_G and $(I_{D3}+I_{D4})/I_G$ showed opposite trends, indicating that there was an optimal operation conditions existed for the reactivity of the coal char. In general, the modification effect of SM coal occurred at λ_P=0.36, T_p=852°C, while that of JC coal and ML coal at λ_P=0.35, T_p=904°C and λ_P=0.38, T_p=899°C, respectively.

Table 4 shows the ultimate and proximate analysis of coal char. According to the ash balance assumption mentioned in Ref. [28], the conversion ratios of each component during preheating were calculated, as shown in Fig. 7. In the preheating process of different coal types, the conversion ratios of volatile and H elements were high, both more than 70%, indicating that in the strong reducing atmosphere, a large amount of volatile was released, and H was more active in partial gasification and combustion reactions. For SM coal and ML coal, due to high volatile content, fuel-N would enter into coal gas with the release of volatile in the preheating process, and the coal char became loose and porous with strong

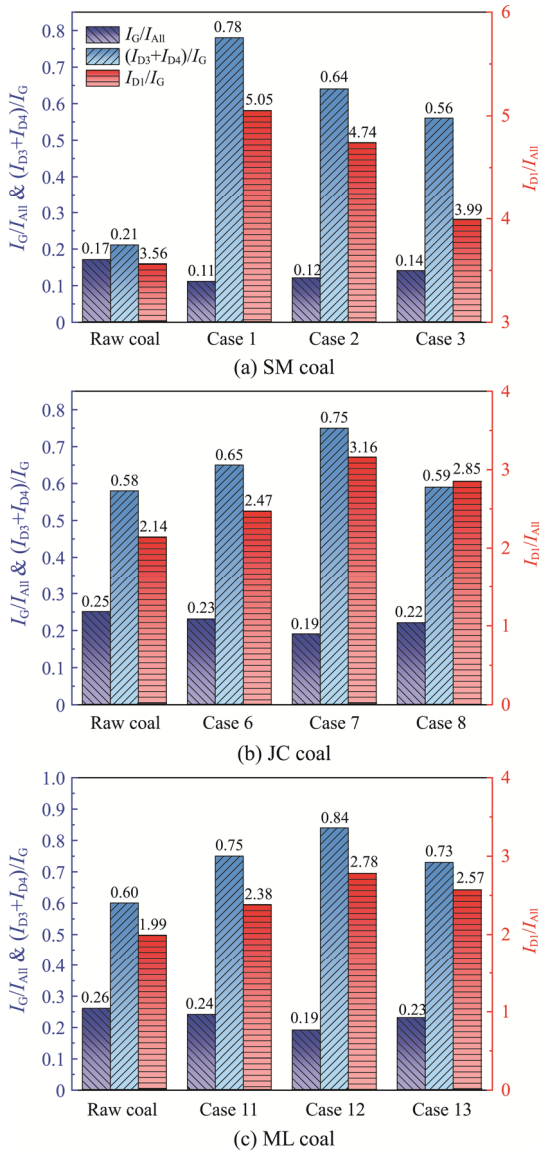

Fig. 6 Variations of band area ratios of raw coal and coal char

reaction activity, resulting in the faster release rate of C, and the conversion ratios of C and N were significantly higher than that of JC coal. With the increase of T_P and λ_P, the conversion ratio of each component of SM coal decreased, while that of ML coal increased. For JC coal, the conversion ratio of each component increased at first and then decreased. Therefore, the appropriate λ_P and T_P should be selected according to the different coal properties, so that the volatile and fuel-N could be released in the self-preheating burner as much as possible, and the released fuel-N was mainly converted into N_2 in the strong reducing atmosphere, thus reducing the total NO_x of the system in the source.

3.1.2 Effects of preheating temperature

The specific surface area, total pore volume and average pore diameter of raw coal and coal char under different T_P are shown in Fig. 8. In all operating conditions, λ_p remains constant, and an auxiliary heater was used to control T_P. With the increase of T_P, the specific surface area, total pore volume and average pore diameter of SM coal char first decreased and then increased, reaching the maximum at about 850°C, while those of JC coal char and ML coal char increased at first and then decreased, reaching the maximum at about 900°C. It could be inferred that the structure of pulverized coal particles could be greatly changed by T_P which exhibited different effects on the particle structure of different coal types. The optimal modification T_P of SM coal emerged at 852°C while that of JC coal and ML coal emerged at 903°C and 900°C, respectively. Through the comparison of Fig. 8 and Fig. 4, although the optimal modification T_P almost did not change, the corresponding specific surface area and pore volume decreased obviously.

Fig. 9 shows variations in band area ratios of raw coal and coal char. With the increase of T_p, I_G/I_{All} of SM coal

Table 4 Ultimate and proximate analysis of coal char

Items	Case 1	Case 2	Case 3	Case 6	Case 7	Case 8	Case 11	Case 12	Case 13
Coal type		SM coal			JC coal			ML coal	
Ultimate analysis/wt% (air dry)									
C	76.45	75.63	81.00	64.72	62.99	61.50	63.05	59.30	56.02
H	1.18	1.43	1.38	0.77	0.63	0.84	1.28	0.94	0.91
O	2.09	3.46	1.69	0.32	0.22	0.54	1.91	1.65	1.42
N	0.78	1.08	0.95	0.60	0.57	0.58	0.72	0.61	0.57
S	0.56	0.55	0.47	2.62	2.55	2.43	0.57	0.63	0.48
Proximate analysis/wt% (air dry)									
M	2.11	1.50	0.91	0.51	1.06	0.67	2.18	0.92	0.51
FC	70.94	63.82	68.82	66.78	64.76	63.76	51.58	52.04	49.10
V	10.12	18.33	16.67	2.25	2.20	2.13	15.95	11.09	10.30
A	16.83	16.35	13.60	30.46	31.98	33.44	30.29	35.95	40.09

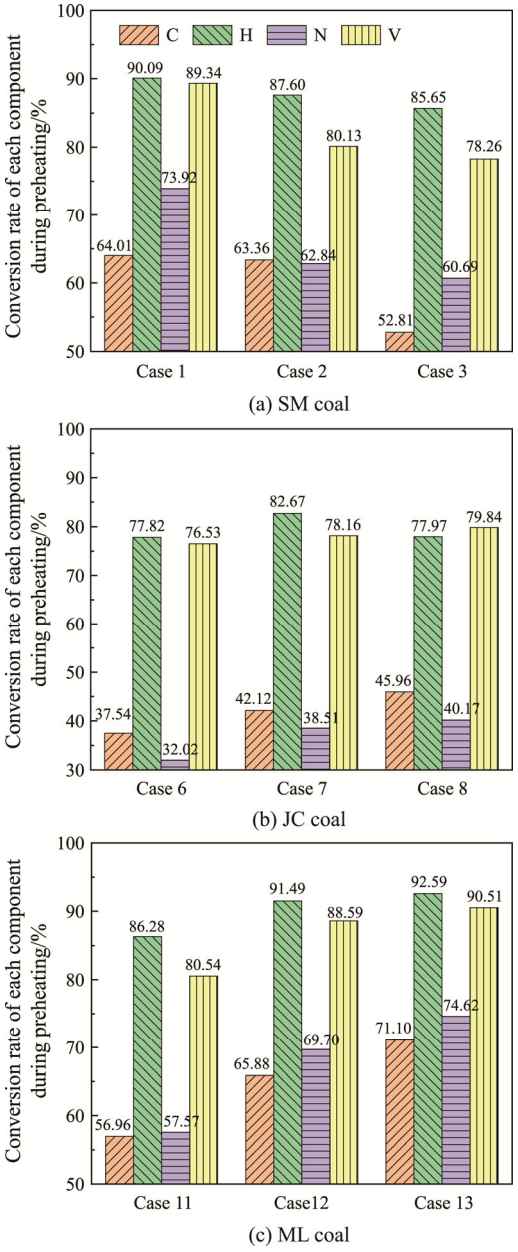

Fig. 7 Conversion ratio of each component after preheating

first increased and then decreased, while I_{D1}/I_G and $(I_{D3}+I_{D4})/I_G$ first decreased and then increased. The graphitization degree reached the maximum at T_p=852°C when the number of active defects was the largest and the proportion of active sites was the largest. The change of carbon structure was consistent with that of particle structure (Fig. 8). With the increase of T_p, I_G/I_{All} of JC coal and ML coal first decreased and then increased, while I_{D1}/I_G and $(I_{D3}+I_{D4})/I_G$ showed opposite trends, indicating that the optimum reaction activity of coal char reached when T_p was about 900°C. By comparing Fig. 9 with Fig. 6, it could be found that the comprehensive effect of coal modification by changing T_p and λ_P was stronger than that by only changing T_p. The reason was that increasing T_p could promote volatile to excrete and promote the formation of pore structure, but at the same time, some volatile would remain on the particle surface and hinder the formation of pore structure. At a certain temperature, the rate of pore formation was equal to the rate of pore reduction. Subsequently, with the increase of T_p, a mounting number of volatile were separated. Under the condition of constant λ_P, the generated substances were not fully taken away, which makes the modification effect of particles worse.

Table 5 shows the ultimate and proximate analysis of coal char. The conversion ratio of each component in the preheating process is shown in Fig. 10. For different coal types, with the increase of T_p, the conversion ratio of

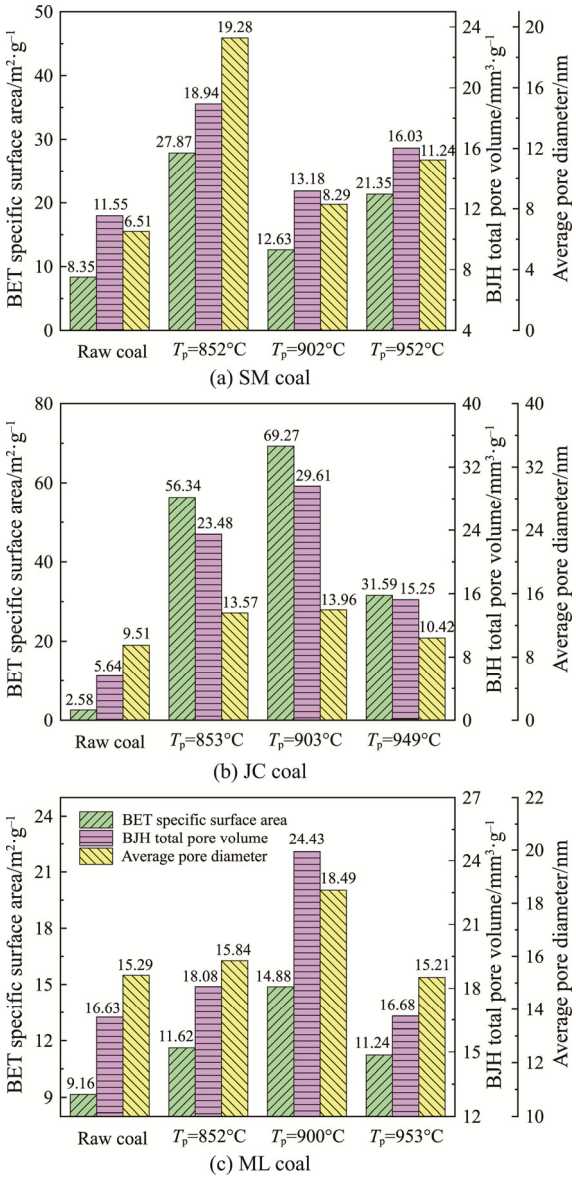

Fig. 8 The specific surface area, total pore volume and average pore diameter of raw coal and char

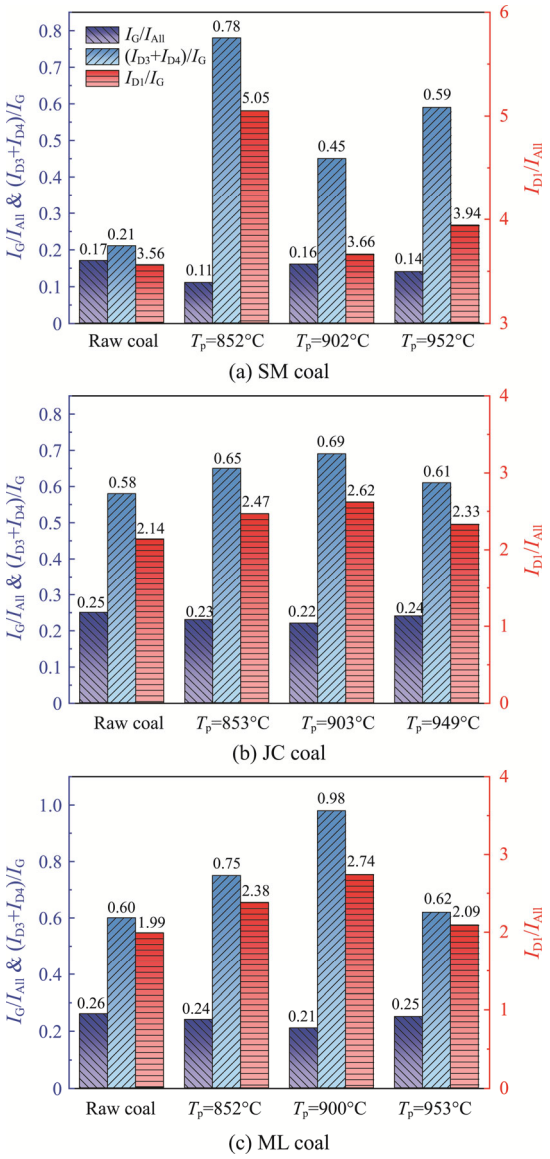

Fig. 9 Variations of band area ratios of raw coal and coal char

each component decreased. Among them, the highest conversion ratio was still the H element, and its conversion ratio was almost over 70%. For the conversion ratio of volatile, SM coal and ML coal were less affected by the rise of T_p, and the range of change was within 10%. At the same time, the volatile conversion ratio of JC was greatly affected by the rise in T_p. With T_p rose from 853°C to 949°C, the conversion ratio of volatile decreased from 76.53% to 55.71%. The minimum conversion ratio of volatile matter of JC coal, which was most affected, was still 55.71%. Although the conversion ratio of volatile matter decreased, it still maintained a relatively high percentage. The conversion ratio of the C element varies among different coals. However, when T_p was only changed for the same coal, the C-element conversion ratio does not change much. The conversion ratio of the N element for SM coal decreased the most, from 73.92% to 56.18%. By comparing Fig. 10 with Fig. 7, it could be found that the conversion ratio of each component of each coal has a downward trend on the whole. The reason may be that the flow velocity of the riser increased with the increase in T_p. The residence time of raw coal in the riser became shorter, which hindered the conversion of internal composition of particles.

3.1.3 Effects of primary air equivalent ratio

The specific surface area, total pore volume, and average pore diameter of raw coal and coal char with different λ_P are shown in Fig. 11. When T_p remained constant, the coal char specific surface area, total pore volume and average pore diameter of JC coal increased with the increase of λ_P, indicating that the increase of λ_P was beneficial to improving the particle structure of coal char, so that more micropores were generated in coal char particles. For SM coal and ML coal, the variation of specific surface area, total pore volume, and average pore diameter with λ_P was greatly affected by T_p.

Table 5 Ultimate and proximate analysis of char

Items	Case 1	Case 4	Case 5	Case 6	Case 9	Case 10	Case 11	Case 14	Case 15
Raw coal		SM coal			JC coal			ML coal	
Ultimate analysis/wt% (air dry)									
C	76.45	74.70	79.86	64.72	65.92	67.47	63.05	62.30	67.02
H	1.18	1.46	1.62	0.77	0.98	1.05	1.28	1.45	1.94
O	2.09	3.77	0.27	0.32	0.65	0.12	1.91	2.79	0.25
N	0.78	1.06	1.23	0.60	0.59	0.62	0.72	0.75	0.82
S	0.56	0.47	0.53	2.62	1.93	2.17	0.57	0.63	0.72
Proximate analysis/wt% (air dry)									
M	2.11	2.21	0.70	0.51	0.43	0.29	2.18	3.55	1.61
FC	70.94	68.73	67.04	66.78	66.79	67.48	51.58	49.67	50.45
V	10.12	12.73	16.47	2.25	3.28	3.95	15.95	18.25	20.30
A	16.83	16.33	15.79	30.46	29.50	28.28	30.29	28.53	27.64

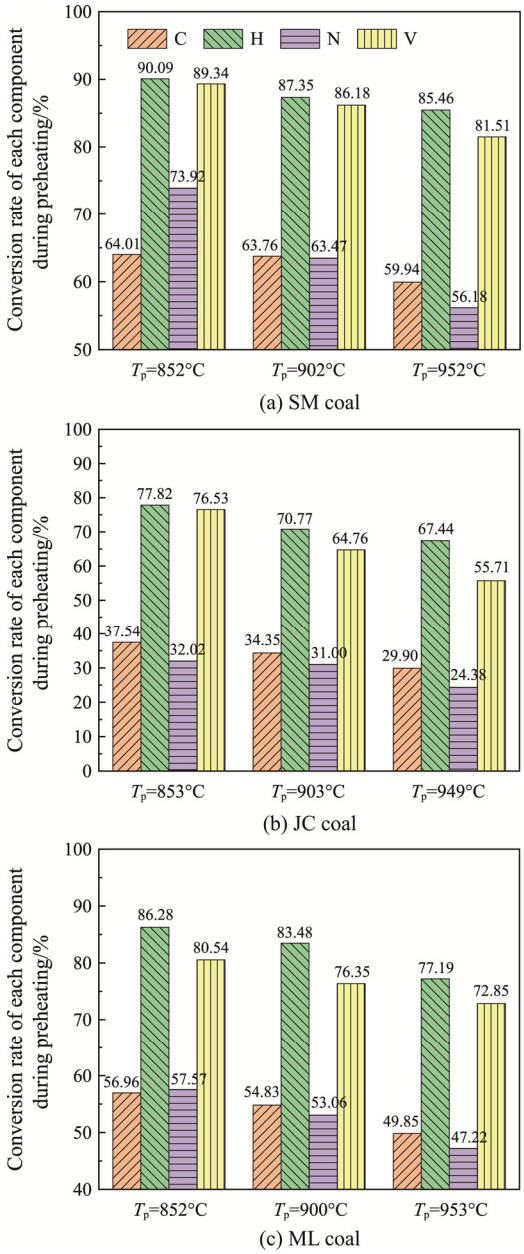

Fig. 10 Conversion ratio of each component after preheating

At T_p≈900°C, the specific surface area, total pore volume, and average pore diameter of SM coal increased with the increase of λ_P but showed opposite trends when T_p further increased to about 950°C. At T_p≈900°C, the specific surface area, total pore volume, and average pore diameter of ML coal decreased with the increase of λ_P, which was not conducive to improving the particle structure of coal char but weakened its reactivity; when T_p further increased to 950°C, the specific surface area, total pore volume, and average pore diameter increased with the increase of λ_P.

Fig. 12 shows variations in band area ratios of raw coal and coal char. For SM coal and ML coal, the relative area ratio of each spectral band varied with λ_P under different T_p. For SM coal, at T_p≈900°C, with the increase of λ_P, I_{D1}/I_G and $(I_{D3}+I_{D4})/I_G$ increased, while I_G/I_{All} decreased, manifesting that both the graphitization degree of carbon structure and the defect density of carbon decreased but the proportion of active centers in the carbon structure increased. And when T_p further increased to about 950°C, with the increase of λ_P, the proportion of active centers in the carbon structure decreased, the defect density of carbon increased, and the reactivity of char remained unchanged. For ML coal, at T_p≈900°C, I_{D1}/I_G increased in the wake of λ_P while I_G/I_{All} dropped in pace with $(I_{D3}+I_{D4})/I_G$ decreased, suggesting that the defect density of carbon augmented and the graphitization degree lessened. At the same time, it also

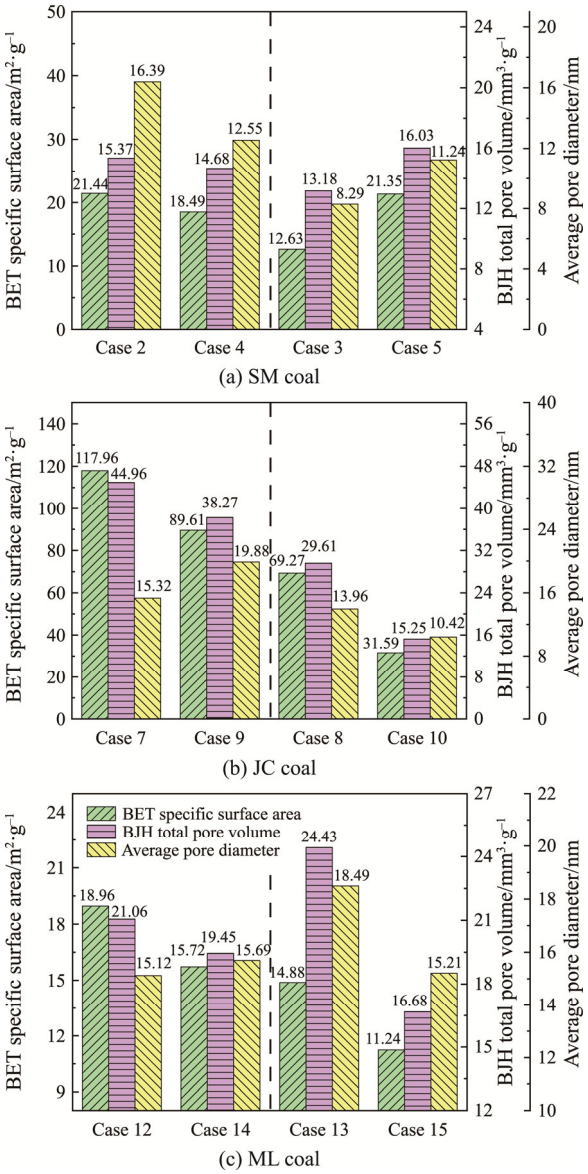

Fig. 11 The specific surface area, total pore volume and average pore diameter of raw coal and coal char

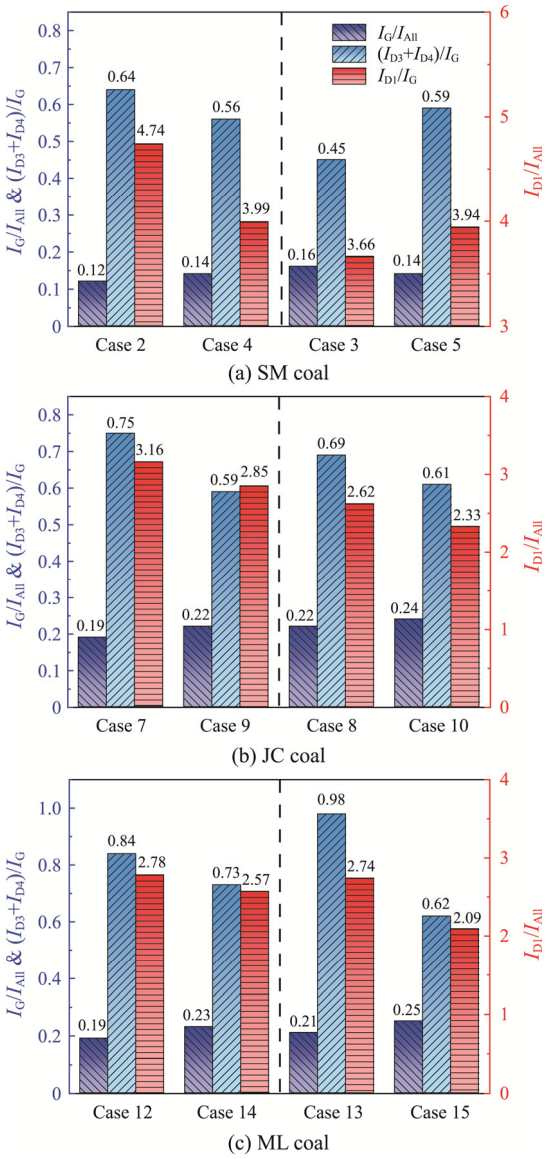

Fig. 12 Raman band relative area ratio of the preheated coal char

indicated the diminution of the proportion of active centers in the carbon structure. When T_p further increased to about 950°C, the proportion of active centers in the carbon structure and the char reactivity increased with the increase of λ_P. For JC coal, with constant T_p, the increase of λ_P was beneficial to improving the particle structure of coal char, promoted the destruction of the stability of graphitization in carbon structure, and enhanced the activity of the particle. By comparing Fig. 12 and Fig. 9, it could be found that for SM coal and ML coal, the effects of changing T_p on the particle structure was higher than that of changing λ_P under certain conditions in this research. It could be inferred that under some certain conditions, T_p played a more significant role in changing the particle structure.

The conversion ratio of each component in the preheating process is shown in Fig. 13. Through comparison, it could be found that in the control group of JC coal and ML coal, the conversion of each component increased with the increasing of primary air equivalent ratio under the condition that T_p was unchanged. The most significant was the control group of ML coal. The T_p of Case 13 and Case 15 were about 950°C, and λ_P of Case 13 was 0.42 while λ_P of Case 15 was 0.33. The C-element conversion ratio of Case 13 was 71.10% while that of Case 15 was 49.85%, and the difference value was 21.25%. As for H element, the conversion ratios were 92.52% and 77.19%, and the former was Case 13. Similarly, the conversion ratio difference for N element was 27.40%, and the conversion ratio for volatile was

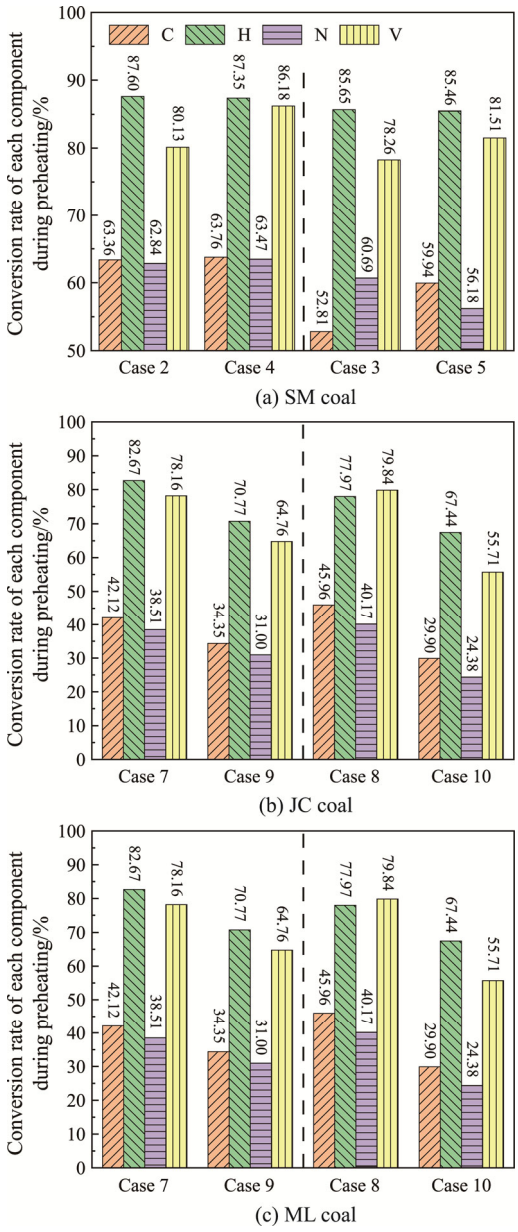

Fig. 13 Conversion ratio of each component after preheating

17.66%. However, according to the control group of SM, the results were different from those of the other two groups. In this control group, the changes in conversion ratios of all components were within 8%. Moreover, at T_p of about 950°C, the conversion ratios of C element and volatiles at the lower air equivalent ratio were higher than that at the higher air equivalent ratio. It could be inferred that a higher λ_P may in some cases promote the conversion of the components. By comparing Fig. 13 and Fig. 10, it could be found that for JC coal and ML coal, the effects of changing λ_P on the conversion ratios of each component was higher than that of changing T_p under certain conditions in this research. It could be inferred that in some cases, λ_P played a more significant role in changing the conversion ratios.

3.2 Coal gas characterization

3.2.1 Comprehensive effects of preheating temperature and primary air equivalent ratio

After entering the self-preheating burner, the pulverized coal will be rapidly heated to above 800°C by the high temperature bed material. In the preheating process, the pulverized coal volatile precipitates and cleaves in a very transitory time to form small molecular gas phase products such as CO, H_2 and CH_4. The chemical reactions are mainly homogeneous and heterogeneous reactions of preheated coal char with oxygen or gas phase (intermediate) products. The main reactions are specifically expressed as [37, 38]:

$C+O_2=CO_2$	–395.1 kJ/mol	(R1)
$C+1/2O_2=CO$	–113.2.1 kJ/mol	(R2)
$CO+1/2O_2=CO_2$	–285.1 kJ/mol	(R3)
$H_2+1/2O_2=H_2O$	–249.0 kJ/mol	(R4)
$CH_4+2O_2=CO_2+2H_2O$	–802.6 kJ/mol	(R5)
$C+CO_2=2CO$	+166.9 kJ/mol	(R6)
$C+H_2O=H_2+CO$	+135.5 kJ/mol	(R7)
$CO+H_2O=CO_2+H_2$	–31.5 kJ/mol	(R8)
$CO+3H_2=CH_4+2O_2$	–227.6 kJ/mol	(R9)

Coal gasification reactions are mainly (R6) and (R7), and the improvement of the quality of the coal gas mainly depends on the strengthening of the two reactions. The energy generated by the process is used to heat the coal and bed material [39–42]. The gas compositions along the riser are shown in Fig. 14. The gas content of the three pulverized coal demonstrated a similar trend except for H_2. CO concentration first decreased and then increased along the axis of the riser, reaching the lowest value at 850 mm from the bottom. The concentration of CH_4 gradually increased, and that of CO_2 did not change much before 850 mm from the bottom, both peaking at 1150 mm before a downward trend. The concentration of O_2 peaked at 850 mm and then decreased with the increase of riser height. As the pulverized coal was added into the dense phase region, it was mainly the heterogeneous reaction of C and O_2 in this region, and the influence of the contact area of fuel and O_2 on the combustion reaction was dominant, so the pulverized coal would be rapidly and violently mixed with the

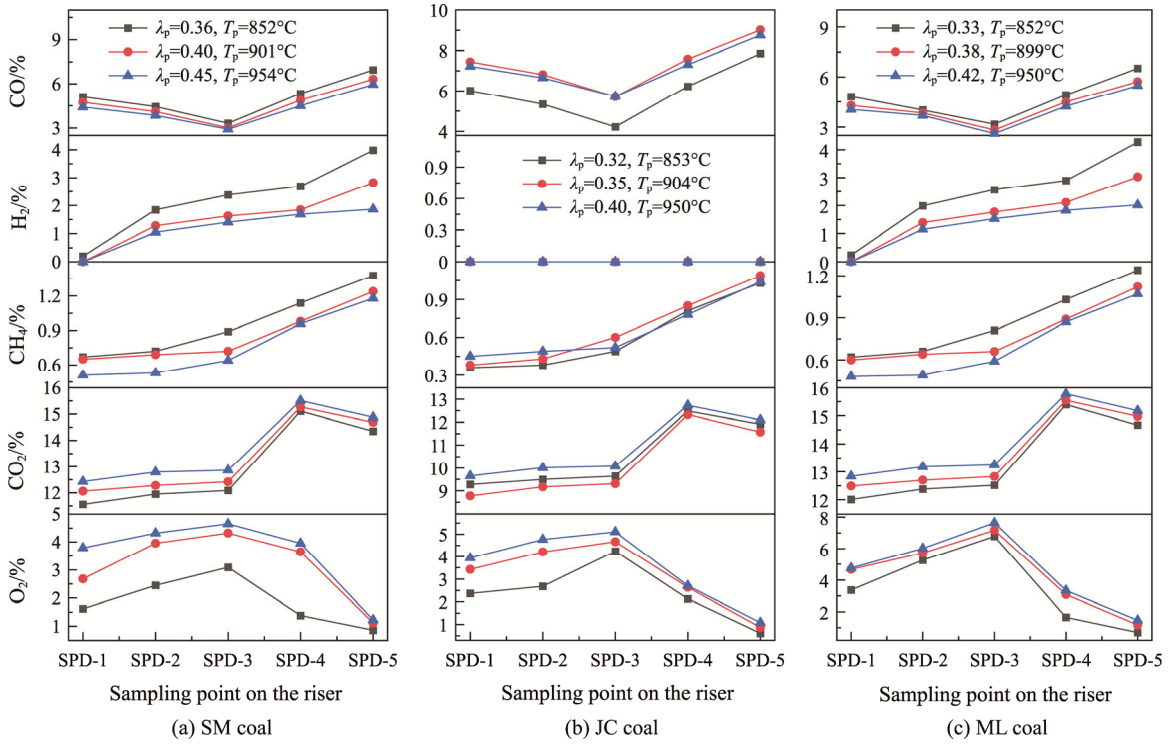

Fig. 14 Coal gas compositions along the axis of the riser

primary air after being added into the self-preheating burner. O_2 was rapidly consumed due to the large contact area. With the gradual generation of gas, the contact area between fuel and O_2 decreased, and the heterogeneous reaction weakened. At this time, oxygen reached its maximum value. With the release of gas components, the homogeneous phase reaction gradually dominated, and the generated combustible gas further consumed O_2. Therefore, taking the maximum O_2 concentration as the boundary, the reaction that occurred above the boundary was the gas in-phase combustion and gasification reaction, while that below the boundary was the gas-solid heterogeneous combustion and gasification reaction. It could be seen that the in-phase reaction was more severe than the gas-solid reaction. For JC coal, due to its lowest volatile content and less H content, the consumption rate of H_2 was higher than the generation rate, so the H_2 concentration was low throughout the route and difficult to be detected. With the increase of λ_P and T_p, the combustion reaction was enhanced while the gasification reaction was weakened.

Fig. 15 shows coal gas compositions at the outlet of the self-preheating burner. With the increase of λ_P and T_p, the content of combustible gas components of SM coal and ML coal decreased, while that of CO_2 increased. In general, the combustion reaction of pulverized coal in the self-preheating burner was strengthened. Nevertheless, the content of combustible gas of JC coal first increased and then decreased, indicating that the gasification reaction was at first intensified by increased temperature, but later the combustion reaction was gradually strengthened by increased O_2 content, while the gasification reaction was weakened. O_2 concentration at the outlet of the self-preheating burner was zero, indicating that there was a strongly reducing atmosphere in the self-preheating burner, which was beneficial to the conversion from fuel-N to N_2.

3.2.2 Effects of preheating temperature

Coal gas compositions along the axis of the riser are shown in Fig. 16. The variation trend of coal gas compositions of the three pulverized coal was roughly similar. For H_2 and CH_4 concentrations, the concentration increased with the elevation of the riser and reached a maximum at 1450 mm. The percentage of CO in the gas decreased first and then increased, reaching the bottom at 850 mm. Moreover, the O_2 content rose before 850 mm, decreased rapidly between 850 mm and 1150 mm, and was almost none at 1450 mm. The concentration of CO_2 increased slightly before 850 mm and there was a relatively major amount of increase between 850 mm and 1150 mm while declined between 1150 mm and 1450 mm. By comparing Fig. 16 with Fig. 14, it could be found that the coal gas trends were a little different. And the relative content of CO, CH_4, and H_2 increased obviously while the content of CO_2 decreased. The trigger was less O_2 content at the same T_p, leading to a stronger reductive atmosphere in comparison to the comprehensive influence of altering T_p and λ_P.

Fig. 17 shows coal gas compositions at the outlet of the self-preheating burner. With the increase of T_p, CO_2 concentration decreased, while that of CO and CH_4 increased. For SM coal and JC coal, the content of H_2 first decreased and then increased, but for ML coal, H_2 monotonically increased with the increase of T_p. H_2 in coal gas mainly came from the polycondensation reaction of the aromatic rings in coal and the water-gas reaction. For ML coal, as T_p increased, the water-gas reaction and pyrolysis reaction were enhanced to promote the generation of H_2, and the volume fraction of H_2 increased.

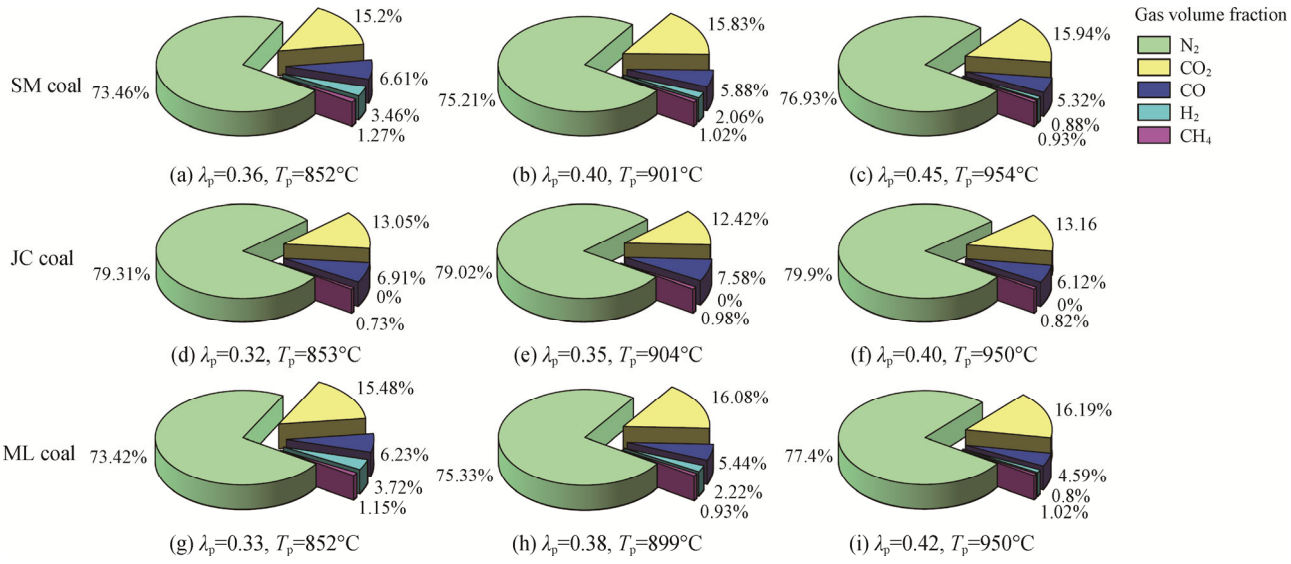

Fig. 15 Coal gas compositions at the outlet of the self-preheating burner

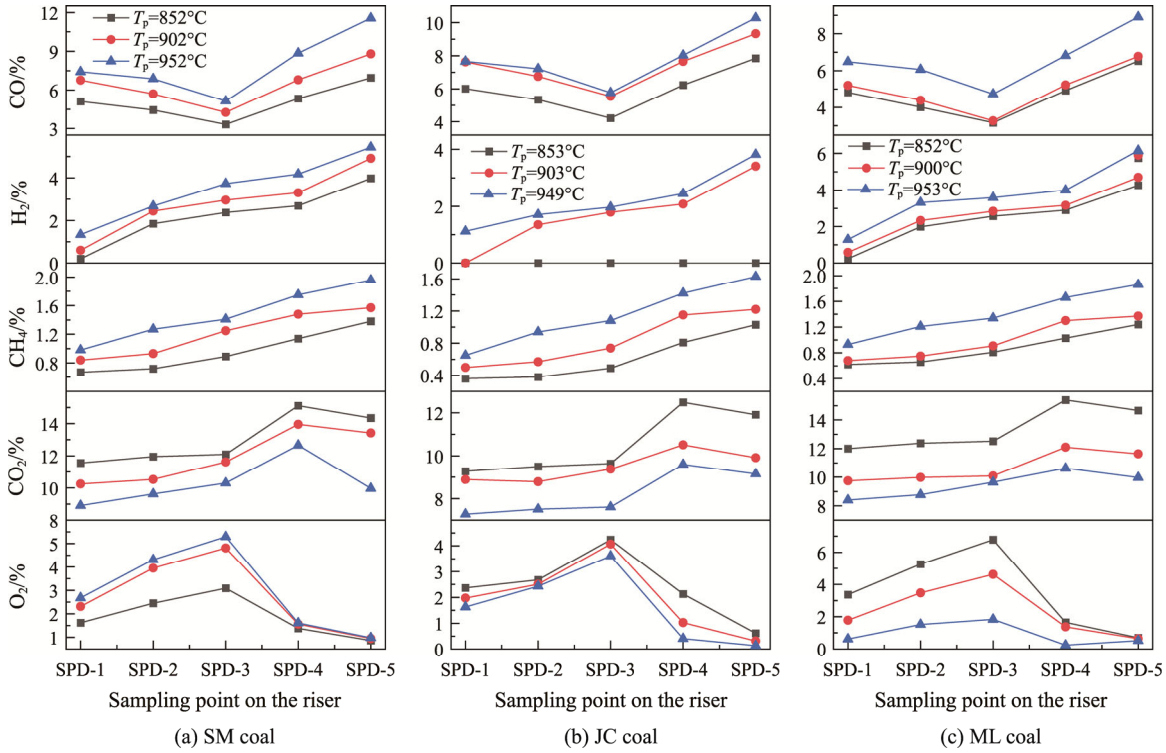

Fig. 16 Coal gas compositions along the axis of the riser

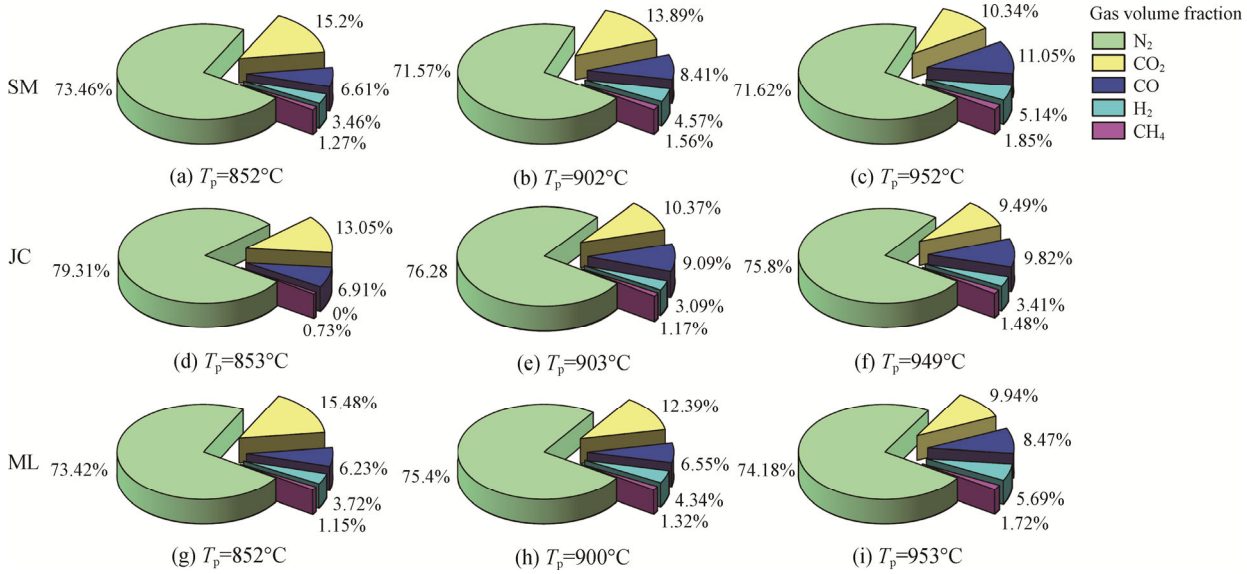

Fig. 17 Coal gas compositions at the outlet of the self-preheating burner

For SM coal and JC coal, as the water-gas reaction was limited by H_2O in coal, with the further increase of T_p, the H_2 oxidation reaction (R3) increased, which was opposite to the water-gas shift reaction (R3). As a consequence, the content of H_2 decreased first and then increased thanks to enhanced water-gas reaction and pyrolysis reaction. CH_4 mainly came from the pyrolysis of the volatile contained in coal. As T_p increased, the pyrolysis reaction was strengthened, and the CH_4 decomposition reaction (R3) reaction rate was reduced, increasing the content of CH_4. By comparing Fig. 17 with Fig. 15, when only T_p was changed, the reducing gas at the outlet of the self-preheating burner accounted for more, which was more conducive to the transformation from fuel-N to N_2.

3.2.3 Effects of primary air equivalent ratio

Fig. 18 shows coal gas compositions along the axis of the riser. When T_p remained constant, with the increase of λ_P, the contents of all combustible gases decreased, while

the CO_2 content increased, illustrating that CO/CO_2 ratio increased with the increase of λ_P, which was beneficial to the exothermic reaction and CO oxidation reaction and further resulted in an increase in the volume fraction of CO_2 in coal gas, a decrease in the volume fraction of CO, an enhanced combustion reaction, and a weakened

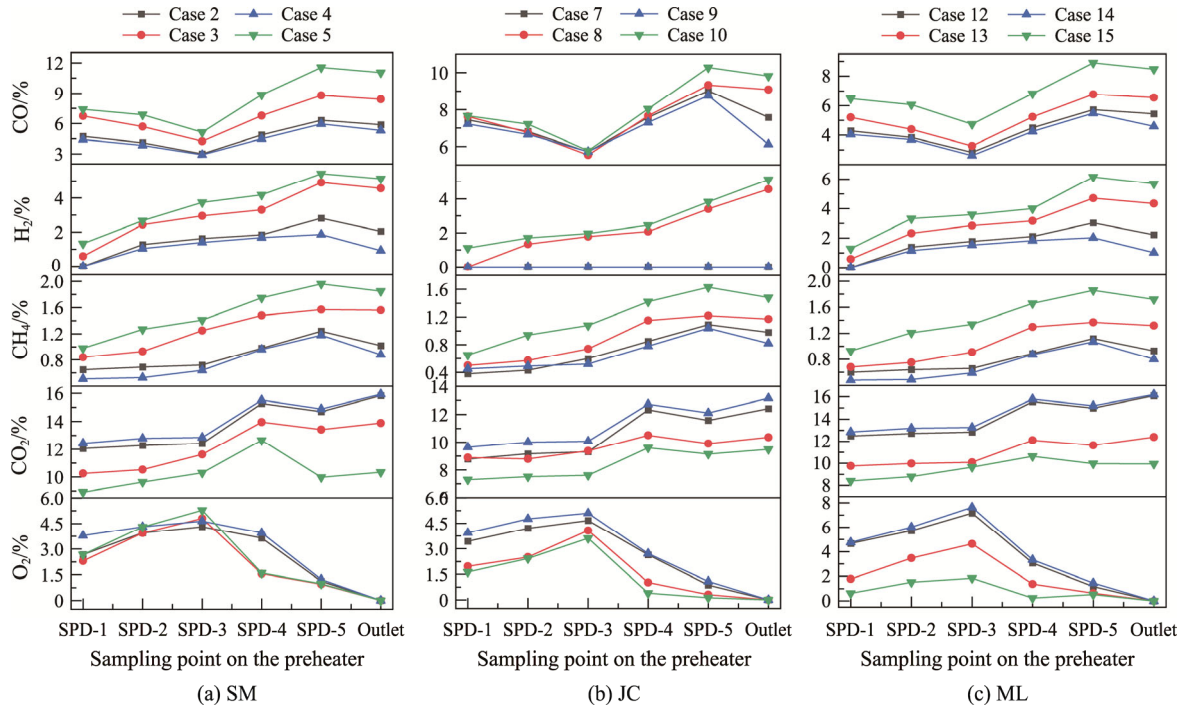

Fig. 18 Coal gas compositions along the axis of the riser

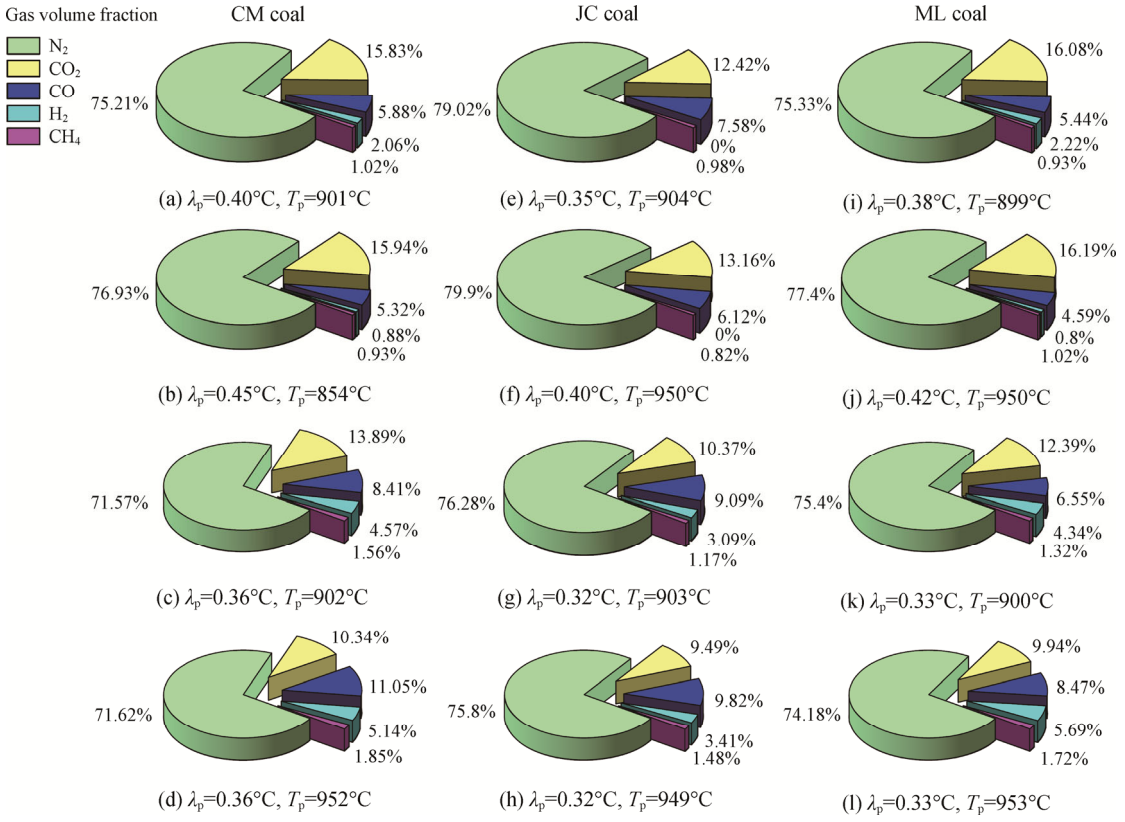

Fig. 19 Coal gas compositions at the outlet of the self-preheating burner

gasification reaction. Additionally, as the fluidization air velocity in the riser increased with the increase of air volume, the residence time of pulverized coal in the riser decreased. As a result, the pyrolysis reaction was weakened, and the contents of H_2, CH_4, and CO produced by pyrolysis were reduced. The increase of O_2 made part of H_2 and CH_4 oxidize (R4) and (R5), which led to the decrease of H_2 and CH_4 volume fractions in coal gas. The above test results were consistent with the results concluded by Zhang et al. [43], but contrary to those by Man et al. [44]. The main reason was that when the former changed O_2/C, T_p only changed slightly. At this time, the oxidation reaction was dominant, which made the volume fraction of CO, H_2, and CH_4 in coal gas decrease. In the latter, T_p changed greatly from 830°C to 940°C when λ_P was changed. At this time, increased T_p resulted in the dominance of pyrolysis reaction and gasification reaction, increasing the volume fraction of CO, H_2, and CH_4 in coal gas.

Fig. 19 shows coal gas compositions at the outlet of the self-preheating burner. With the increase of λ_P, CO_2 concentration increased, while that of CO, H_2 and CH_4 decreased. By comparing with Fig. 18, it could be found the effects of increasing primary air equivalent ratio on reducing gas composition were exactly opposite to that of increasing T_p. The reason may be that more air provided more O_2, making the oxidation reaction more intense. Moreover, increasing the air equivalent ratio directly increased the primary air velocity, which shortened the time of particles in the riser and reduced the amount of reduced material precipitated.

3.3 Coal tar characterization

3.3.1 Comprehensive effects of preheating temperature and primary air equivalent ratio

Coal tar was collected at the outlet of the self-preheating burner. The flue gas was passed through an ice water bath equipped with isopropanol to obtain the tar-isopropanol mixture liquid containing coal char. And then, the coal char was removed by filtration to obtain the clear tar-isopropanol mixture solution.

The tar amount and yield at the outlet of the self-preheating burner are shown in Fig. 20. The definition of tar amount (M_{tar}) was the weight of tar remained after isopropanol was evaporated in tar-isopropanol mixture solution by the rotary evaporator under the water bath condition of 40°C.

The amount of tar produced by coal preheating was calculated as Eqs. (1) and (2).

$$M_{tar}=m_{tar}\cdot(V_{total}/V_{collet}) \quad (1)$$

$$V_{collet}=P_{pump}\cdot t_{collet} \quad (2)$$

where M_{tar} (kg/h) represents the weight of tar collected in one hour; m_{tar} (kg) represents the tar weight contained in the flue gas collected at a certain time; V_{total} (L/h) represents volume of the fuel gas produced per hour; V_{collet} (L) represents the volume of flue gas entered through isopropanol; P_{pump} (L/h) represents the power of the vacuum pimp; t_{collet} (h) represents the pumping time of vacuum pump.

The yields of tar produced by coal preheating are calculated as Eq. (3).

$$Y_{tar}=M_{tar}/M_{coal}\cdot 100\% \quad (3)$$

where Y_{tar} (%) represents tar yield; M_{coal} (kg/h) represents the fuel feed rate.

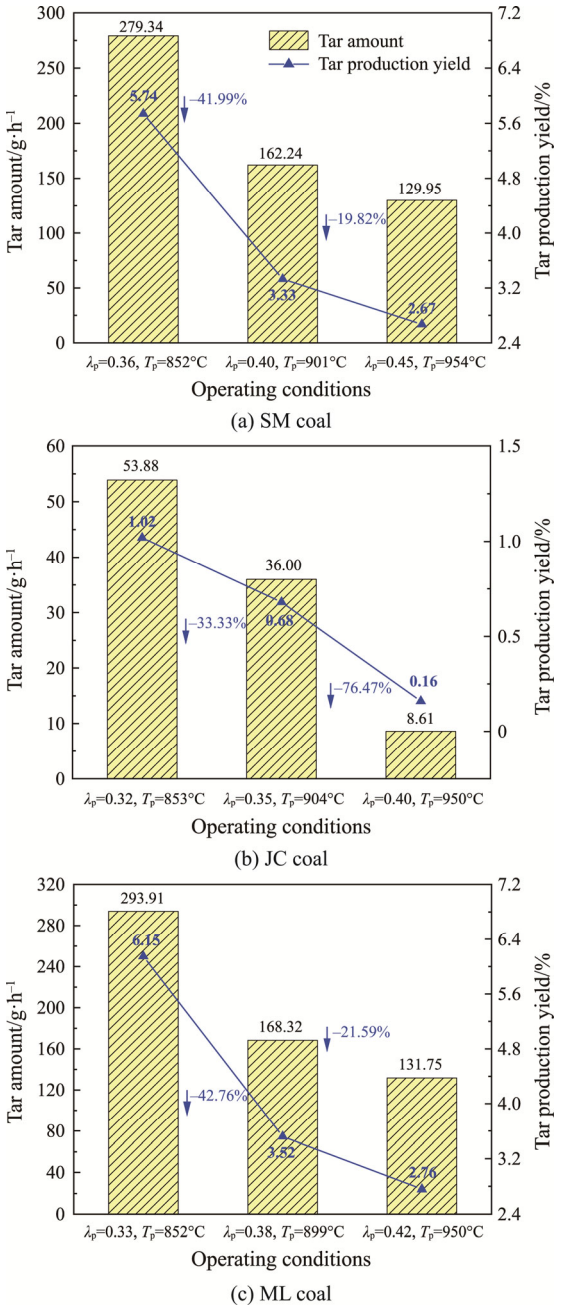

Fig. 20 The mount and the production yield of coal tar at the outlet of the self-preheating burner

Due to the low volatile content, the coal tar amount and the production yield of JC coal were significantly lower than those of SM coal and ML coal, and it could be inferred that when λ_P>0.40 and T_p>950°C, it was difficult to extract coal tar from the outlet of self-heating burner for JC coal. Regarding SM coal and ML coal, due to the high volatile content, a large amount of coal tar would be generated in the preheating process at 850°C, with coal tar production yield of up to 5.74% and 6.15%, respectively, indicating that T_p=850°C was conducive to the formation of coal tar. With the increase of λ_P and T_p, the amount and the production yield of coal tar decreased significantly. In particular, when T_p increased from 850°C to 900°C, the coal tar production yield decreased by almost 50%. Since coal tar was essentially a fragment of macromolecular structure in coal, it was produced in the initial stage of coal volatilization and had high reaction activity. The increase of λ_P and T_p further promoted the secondary cracking and oxidation of coal tar [45, 46]. With the increase of T_p, the coal tar production yield of SM coal decreased less significantly than that of JC coal, indicating that coal tar produced by SM coal had higher thermal stability. The difference between coal tar production yield and coal tar loss rate with the increase of λ_P and T_p was due to the different aromatics structures of coal.

To further illustrate the coal tar formation mechanism of the self-preheating burner under different operating conditions, the composition and content of coal tar at the outlet of the self-preheating burner were analyzed by gas chromatography-mass spectrometry (GC-MS). Taking the working conditions of SM coal as an example, the specific composition of coal tar under Cases 1–3 are shown in Table 6, Table 7, and Table 8 respectively. Thus it could be seen that coal tar components were mainly aromatic compounds.

The tar obtained under case 1, case 2, and case 3 each contained some different substances. For $C_xH_yO_xSi_z$, λ_p and T_p increased while the relative amount of $C_xH_yO_xSi_z$ was drastically reduced. The relative amount of case 1, case 2, and case 3 were 13.08%, 6.27%, and 1.05%, respectively, indicating that $C_xH_yO_xSi_z$ was greatly affected by changing λ_p and T_p. The reason may be that such macromolecular substances rapidly decomposed into smaller and more stable molecular structures as the temperature rose and converted silicon from an elemental state to other forms. Moreover, the tar obtained under Case 1 and Case 2 contained the roughly same N substance, which was mainly triazine compound 1H-1,2, 4-triazole-3-carboxylic acid ($C_3H_3N_3O_2$), with a relative content of 8.84% and 19.80%, respectively. Under Case 3, the relative content of N in tar decreased significantly, mainly 2,3,5,6-Dibenzo-7,8-diazabicyclo<2.2.2>octamer-2,5-diene ($C_{14}H_{12}N_2$) and (9Z)-9-hexadecenamide ($C_{16}H_{31}NO$), which were 1.46% and 2.66%, respectively. The reason may be that when λ_p

Table 6 Coal tar composition and relative content in Case 1 (λ_p=0.36, T_p=852°C)

Number	Retention time/min	Compound name	Chemical formula	Relative amount/%
1	2.524	2-Pentanone	$C_5H_{10}O$	9.01
2	2.568	1H-1,2, 4-triazole-3-carboxylic acid	$C_3H_3N_3O_2$	8.84
3	2.885	Acetal	$C_6H_{14}O_2$	1.00
4	2.987	4-Methyl-2-pentanone	$C_6H_{12}O$	2.00
5	3.306	Toluene	C_7H_8	23.35
6	4.646	O-xylene	C_8H_{10}	2.33
7	4.962	Styrene	C_8H_8	1.66
8	5.010	m-xylene	C_8H_{10}	0.95
9	6.507	2,2-Dimethyldecane	$C_{12}H_{26}$	2.15
10	7.421	1-Chlorindan	C_9H_9Cl	1.71
11	9.632	Azulene	$C_{10}H_8$	2.73
12	14.019	2,4-Di-tert-butylphenol	$C_{14}H_{22}O$	3.66
13	23.227	2,2′-Methylenebis-(4-methyl-6-tert-butylphenol)	$C_{23}H_{32}O_2$	9.99
14	24.212	octadecamethylcyclononasiloxane	$C_{18}H_{54}O_9Si_9$	7.67
15	24.697	Hexamethylheptasiloxane	$C_{16}H_{48}O_6Si_7$	0.89
16	25.904	Erucamide	$C_{22}H_{43}NO$	2.97
17	32.295	Decamethyldihydropentasiloxane	$C_{10}H_{32}O_4Si_5$	2.24
18	32.435	(diethoxy-trimethylsilyloxysilyl) oxy-trimethylsilane	$C_{10}H_{28}O_4Si_3$	1.56
19	32.592	Antioxidant 1076	$C_{35}H_{62}O_3$	12.54
20	32.685	(diethoxy-trimethylsilyloxysilyl) oxy-trimethylsilane	$C_{10}H_{28}O_4Si_3$	0.72

Table 7 Coal tar composition and relative content in Case 2 (λ_p=0.40, T_p=901°C)

Number	Retention time/min	Compound name	Chemical formula	Relative amount/%
1	2.524	2-Pentanone	$C_5H_{10}O$	10.98
2	2.570	1H-1,2, 4-triazole-3-carboxylic acid	$C_3H_3N_3O_2$	19.80
3	2.987	4-Methyl-2-pentanone	$C_6H_{12}O$	2.31
4	3.305	Toluene	C_7H_8	26.50
5	4.645	m-xylene	C_8H_{10}	2.17
6	6.506	2,2-Dimethyldecane	$C_{12}H_{26}$	2.65
7	9.633	Azulene	$C_{10}H_8$	3.44
8	14.021	2,4-Di-tert-butylphenol	$C_{14}H_{22}O$	3.43
9	23.088	octadecamethylcyclononasiloxane	$C_{18}H_{54}O_9Si_9$	3.21
10	23.227	2,2′-Methylenebis-(4-methyl-6-tert-butylphenol)	$C_{23}H_{32}O_2$	9.15
11	25.904	Erucamide	$C_{22}H_{43}NO$	3.21
12	27.160	Ecosamethylcyclodecasiloxane	$C_{20}H_{60}O_{10}Si_{10}$	3.06
13	32.590	Antioxidant 1076	$C_{35}H_{62}O_3$	9.70

Table 8 Coal tar composition and relative content in Case 3 (λ_p=0.45, T_p=954°C)

Number	Retention time/min	Compound name	Chemical formula	Relative amount/%
1	2.564	1-Methoxy-2-propanone	$C_4H_8O_2$	12.42
2	3.161	4-Methyl-2-pentanone	$C_6H_{14}O$	17.77
3	3.305	Toluene	C_7H_8	17.19
4	4.642	O-xylene	C_8H_{10}	0.97
5	4.741	Phenylacetylene	C_8H_6	1.34
6	4.962	Styrene	C_8H_8	2.43
7	6.506	2,2-Dimethyldecane	$C_{12}H_{26}$	1.21
8	7.419	1-Chlorindan	C_9H_9Cl	3.27
9	9.630	Azulene	$C_{10}H_8$	12.88
10	10.899	3,8-Dimethyl-undecane	$C_{13}H_{28}$	0.47
11	13.405	Biphenylene	$C_{12}H_8$	3.09
12	14.020	2,4-Di-tert-butylphenol	$C_{14}H_{22}O$	2.18
13	17.382	2,3,5,6-Dibenzo-7,8-diazabicyclo<2.2.2> octamer-2,5-diene	$C_{14}H_{12}N_2$	1.46
14	20.289	Fluoranthene	$C_{16}H_{10}$	1.08
15	23.229	2,2′-Methylenebis-(4-methyl-6-tert-butylphenol)	$C_{23}H_{32}O_2$	7.49
16	25.261	octadecamethylcyclononasiloxane	$C_{18}H_{54}O_9Si_9$	1.05
17	25.905	(9Z)-9-hexadecenamide	$C_{16}H_{31}NO$	2.66
18	32.590	Antioxidant 1076	$C_{35}H_{62}O_3$	8.90

increased from 0.36 to 0.40 and T_p increased from 852°C to 901°C, the migration of fuel N to tar N was promoted. And when λ_p increased from 0.40 to 0.45, and T_p increased from 901°C to 954°C, the nitrogen compounds in tar were significantly reduced, and a large amount of them was decomposed and converted into NH_3 and N_2. Meanwhile, the relative amount of hydrocarbons (C_xH_y) in Case 1, Case 2, and Case 3 are 33.17%, 34.76%, and 40.66%, respectively. It could be seen from the above that the relative amount of hydrocarbons was relatively stable and showed a small upward trend, indicating that such substances were relatively less affected.

3.3.2 Effects of preheating temperature

Fig. 21 showed the amount and the production yield of coal tar under different preheating temperatures. The coal tar production yield of JC coal at 949°C was only 0.37%, making it difficult to extract from export. Due to the high volatile content of SM coal and ML coal, a large amount of coal tar was produced in the preheating process at about 850°C, with the production yield being up to 5.74% and 6.15%, respectively, indicating that T_p=850°C was conducive to the formation of coal tar. With the increase of T_p, both the amount and the production yield of coal tar decreased significantly. For SM coal, when T_p

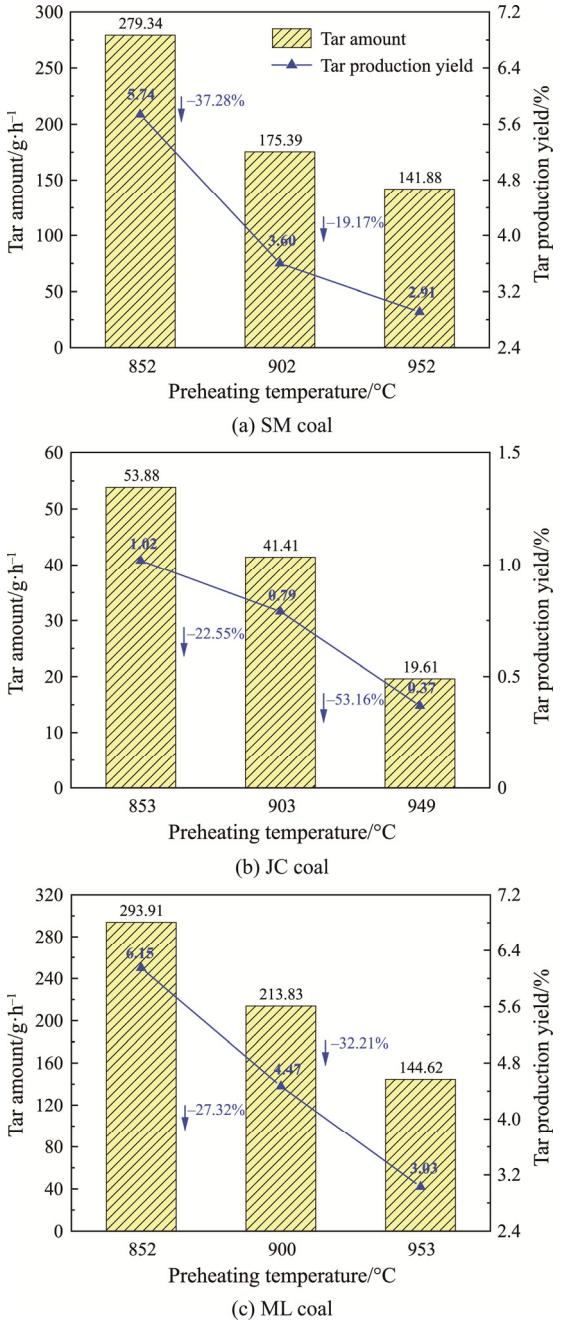

Fig. 21 The amount and the production yield of coal tar at the outlet of the self-preheating burner

increased from 850°C to 900°C, the coal tar production yield decreased rapidly, by 37.28%, and the coal tar thermal stability was poor For ML coal; the coal tar production yield decreased approximately linearly with the increase of T_p. By comparing Fig. 21 with Fig. 20, it could be found that the rate of decline in coal tar production yield had slowed down on the whole.

3.3.3 Effects of primary air equivalent ratio

Fig. 22 showed the amount and the production yield of coal tar under different primary air equivalent ratios. It could be intuitively compared through Fig. 22, a rise in λ_p would lead to a fall in tar yield. The cause may be that in the high-temperature condition, increasing λ_p would make the tar attached to the surface of the coal coke leave the solid particles, increase the contact area with the gas and promote the tar decomposition. In addition, with the increase in primary air equivalent ratio, the O_2 flowing into the primary air increased, and part of the tar reacted with the O_2 in the primary air, resulting in the reduction of tar yield. Besides, due to the low volatile content of JC coal, when the T_p was 949°C, the tar yield was only

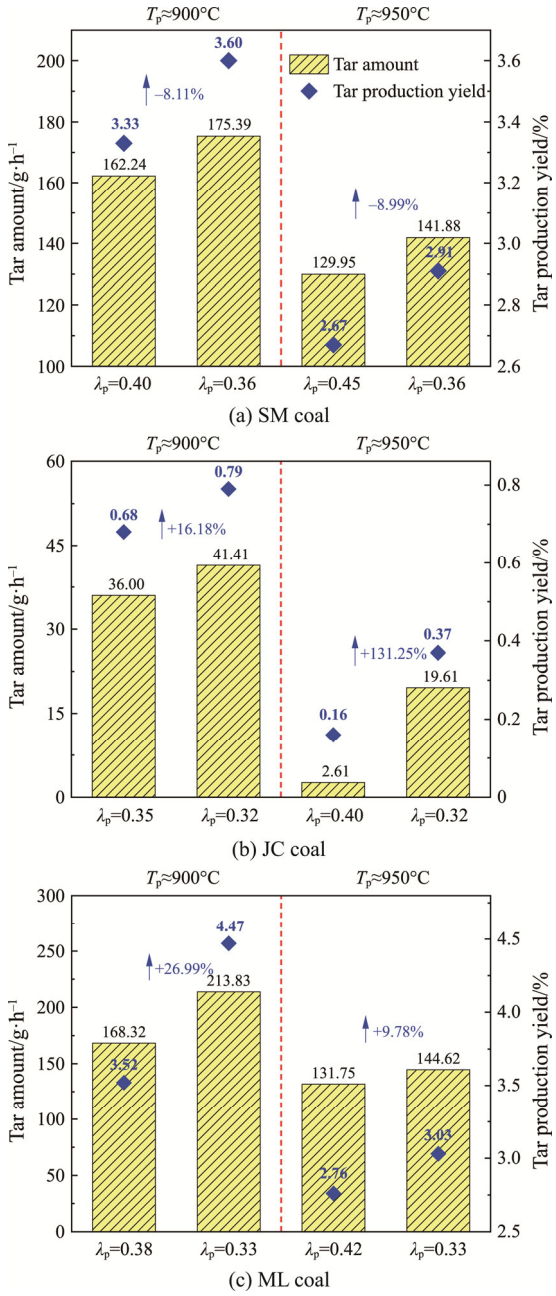

Fig. 22 The amount and the production yield of coal tar at the outlet of the self-preheating burner

0.37%. It was inferred that it would be difficult to extract tar at the preheater outlet under higher temperatures. In addition to T_p and λ_p having a great influence on the tar yield, it was confirmed again that different coal types also had a great influence on the tar yield.

4. Conclusion

A bench test was carried out on the preheating characteristics of coal to study the comprehensive effects of changing T_p and λ_p simultaneously, and the influence of single variable of T_p and λ_p on the fuel preheating characteristics were also accurately analyzed. The results were summarized as follows.

When changed both T_p and λ_p, the optimal modification effect of SM emerges at λ_p=0.36, T_p=852°C, while those of JC and ML emerge at λ_p=0.35, T_p=904°C, and λ_p=0.38, T_p=899°C, respectively. When changing T_p only, the optimal modification effect of SM occurs at T_p=852°C, and those of JC and ML occur at T_p=903°C and T_p=900°C, respectively. When changing λ_p, the specific surface area, total pore volume, and average pore size of char increased with the increase of λ_p. In this research, changing T_p had a greater effect on the particle structure than changing λ_p under these experimental conditions. At the same time, under certain conditions, the effects of λ_p on the conversion of each component were greater than that of T_p.

With the increase in T_p and λ_p, the combustion reaction was enhanced while the gasification reaction was weakened, which was beneficial to the conversion of N to N_2 after precipitation. At the same λ_p, with the increase in T_p, the gasification reaction was strengthened while the combustion reaction was weakened, which was beneficial to the conversion of N to N_2 after precipitation. At the same T_p, with the increase of λ_p, the combustion reaction was enhanced while the gasification reaction was weakened. In addition, as a result of the weakened pyrolysis reaction, the contents of H_2, CH_4 and CO produced by pyrolysis decreased, resulting in a decrease in the volume fraction of H_2 and CH_4 in the gas.

In the preheating process of anthracite, a very small amount of each component was transferred to tar, and the volatile was dominated by high-temperature gas. The difference between tar yield and tar loss rate with the increase in λ_p and T_p was caused by the difference in aromatic structure between coals.

Acknowledgment

This study was supported by CAS Project for Young Scientists in Basic Research (YSBR-028), Strategic Priority Research Program of the Chinese Academy of Sciences (XDA21040100) and Youth Innovation Promotion Association of the Chinese Academy of Sciences (2019148).

Conflict of Interest

On behalf of all authors, the corresponding author states that there is no conflict of interest.

References

[1] Wang J., Fan W., Li Yu, Xiao M., Wang K., Ren P., The effect of air staged combustionon NO_x emissions in dried lignite combustion. Energy, 2012, 37(1): 725–736.

[2] Li Z., Liu G., Zhu Q., Chen Z., Ren F., Combustion and NO_x emission characteristics ofa retrofitted down-fired 660A MWe utility boiler at different loads. Applied Energy, 2011, 88(7): 2400–2406.

[3] Kuang M., Li Z., Zhang Y., Chen X., Jia J., Zhu Q., Asymmetric combustion characteristics and NO_x emissions of a down-fired 300 MWe utility boiler at different boiler loads. Energy, 2012, 37(1): 580–590.

[4] National Bureau of Statistics of China., Statistical bulletin of the people's republic of China on national economic and social development in 2021. People's Daily, 2022-03-01(010).

[5] Qian B., China's coal chemical industry development prospects. Shanghai Chemical Industry, 2015, 40(1): 33–38.

[6] Wang C., Wang F., Ye Y., Zhang X., Su Y., Jiang L., Li Z., Zhang H., Evolving characteristics and driving mechanism of coal consumption in China based on the perspective of supply and demand. Journal of Natural Resources, 2020, 35(11): 2708–2723.

[7] Bamminger C., Poll C., Marhan S., Offsetting global warming-induced elevated greenhouse gas emissions from an arable soil by biochar application. Global Change Biology, 2018, 24(1): 318–334.

[8] Bongaarts J., Intergovernmental panel on climate change special report on global warming of 1.5°C Switzerland: IPCC, 2018. Population and Development Review, 2019, 45(1): 251–252.

[9] Sang S., Wand R., Zhou X., Huang H., Liu S., Han S., Review on carbon neutralization associated with coal geology. Meitiandizhi Yu Kantan/Coal Geology and Exploration, 2021, 49(1): 1–11. (in Chinese)

[10] Lu Q., Zhu J., Niu T., et al., Pulverized coal combustion and NO_x emissions in high temperature air from circulating fluidized bed. Fuel Processing Technology, 2008, 89(11): 1186–1192.

[11] Wang J., Experimental study on preheating combustion and NO_x generation of anthracite in circulating fluidized bed. Graduate University of Chinese Academy of

Sciences, Institute of Engineering Thermophysics, Beijing, China, 2011.

[12] Ouyang Z., Zhu J., Lu Q., Experimental study on preheating and combustion characteristics of pulverized anthracite coal. Fuel, 2013, 113: 122–127.

[13] Ouyang Z., Particle characteristics of anthracite powder preheated quickly in circulating fluidized bed. 2013 International Conference on Materials for Renewable Energy and Environment, Chengdu, China, 2014, 1(3):796–801.

[14] Zhu S., Lyu Q., Zhu J., et al., Experimental study on pulverized char combustion preheated by a circulating fluidized bed. Journal of Engineering Thermophysics, 2018, 39(4): 887–892.

[15] Zhu S., Zhu J., Lyu Q., et al., Pilot-scale study on NO emissions from coarse coal combustion preheated by circulating fluidized bed. Fuel, 2020, 280: 118563.

[16] Zhang Y., Zhu J., Lyu Q., et al., Experiment on preheating characteristics of bituminous coal by circulating fluidized bed. China Powder Science and Technology, 2019, 25(6): 5.

[17] Zhang Y., Zhu J., Lyu Q., et al., Coke generation and conversion behavior of pulverized coal combustion. Journal-Energy Institute, 2020, 93(5): 2096–2107.

[18] Zhang Y., Zhu J., Lyu Q., et al., The ultra-low NO_x emission characteristics of pulverized coal combustion after high temperature preheating. Fuel, 2020, 277: 118050.

[19] Ding H., Ouyang Z., Zhang X., et al., The effects of particle size on flameless combustion characteristics and NO emissions of semi-coke with coal preheating technology. Fuel, 2021, 297(1): 120758.

[20] Zhang X., Zhu S., Song W., et al., Experimental study on conversion characteristics of anthracite and bituminous coal during preheating-gasification. Fuel, 2022, 324: 124712.

[21] Su K., Ding H., Ouyang Z., Zhang J., Experimental study on effects of multistage reactant and air jet velocities on self-preheating characteristics and NO_x emission of burning pulverized coal. Fuel, 2022, 325: 124879.

[22] Ouyang Z., Ding H., Liu W., Li S., Cao X., Effect of the staged secondary air on NO_x emission of pulverized semi-coke flameless combustion with coal preheating technology. Fuel, 2021, 291: 120137.

[23] Ouyang Z., Liu W., Man C., Zhu J., Liu J., Experimental study on combustion flame and NO_x emission of pulverized coal preheated by a preheating burner. Fuel Processing Technology, 2018, 179: 197–202.

[24] Ouyang Z., Ding H., Liu W., Cao X., Zhu S., Effect of the primary air ratio on combustion of the fuel preheated in a self-preheating burner. Combustion Science and Technology, 2022, 194(6): 1247–1264.

[25] Liu W., Ouyang Z., Song W., Zhu S., Li S., Experimental research on combustion characteristics and NO_x emission of three kinds of solid fuels preheated by a self-Preheating burner. Energy & Fuels, 2019, 33(9): 8483-8490.

[26] Liu W., Ouyang Z., Cao X., Na Y., Liu D., Zhu S., Effects of secondary air velocity on NO emission with coal preheating technology. Fuel, 2019, 256: 115898.

[27] Liu W., Ouyang Z., Cao X., Na Y., The influence of air-stage method on flameless combustion of coal gasification fly ash with coal self-preheating technology. Fuel, 2019, 235: 1368–1376.

[28] Ouyang Z., Experimental study on preheating, Combustion and pollutant formation of anthracite powder. University of Chinese Academy of Sciences, Institute of Engineering Thermophysics, Beijing, China, 2014.

[29] Yao Y., Experimental study on preheating combustion and NO_x formation of semi-coke powder. University of Chinese Academy of Sciences, Institute of Engineering Thermophysics, Beijing, China, 2016.

[30] Sheng C.D., Char structure characterized by Raman spectroscopy and its correlations with combustion reactivity. Fuel, 2007, 86: 2316–2324.

[31] Beyssac O., Coffe B., Petitet J.-P., Froigneux E., Moreau M., Rouzaud J-N., On the characterisation of disordered and heterogeneous carbonaceous materials by Raman spectroscopy. Spectrochimica Acta Part A, 2003, 59: 2267–2276.

[32] Zaida V., Bar-Ziv E., Radovic LR., Lee Y-J., Further development of Raman microprobe spectroscopy for characterization of char reactivity. Proceedings of the Combustion Institute, 2006, 31: 1873–1880.

[33] Li X., Hayashi J., Li C., FT-Raman spectroscopic study of the evolution of char structure during the pyrolysis of a Victorian brown coal. Fuel, 2006, 85: 1700–1707.

[34] Liu X., You J., Wang Y., et al., Raman spectroscopic study on the pyrolysis of Australian bituminous coal. Journal of Fuel Chemistry and Technology, 2014, 42(3): 270–276.

[35] Zhang Y., Zhu J., Lyu Q., Pan F., Experimental study on combustion characteristics of pulverized coal based on partial gasification of circulating fluidized bed. Energy & Fuels, 2019, 34(1): 989–995.

[36] Zhang Y., Zhu J., Lyu Q., Pan F., Zhu S., Characteristics of preheating combustion of power coal with high coking properties. Journal of Thermal Science, 2021, 30(4): 1108–1115.

[37] Liu J., Zhu Z., Jiang H., Gasification of bituminous coal in a dual-bed system at different air/coal ratios. Energy & Fuels, 2015, 29(2): 496–500.

[38] Liang C., Lyu Q., Zhang H., et al., Experimental investigation of circulating fluidized bed gasification in O_2-enriched air and steam. Journal of Combustion Science and Technology, 2019, 25(02): 105–111.

[39] Zhu S., Lyu Q., Zhu J., Experimental investigation of NO_x emissions during pulverized char combustion in oxygen-enriched air preheated with a circulating fluidized bed. Journal of the Energy Institute, 2019, 92(5): 1388–1398.

[40] Zhu S., Lyu Q., Zhu J., Wu H., Wu G., Effect of Air Distribution on NO_x. Emissions of pulverized coal and char combustion preheated by a circulating fluidized bed. Energy & Fuels, 2018, 32(7): 7909–7915.

[41] Zhu S., Lyu Q., Zhu J., Wu H., Fan Y., Low NO_x emissions from pulverized coal moderate or intense low-oxygen dilution combustion in O_2/CO_2 preheated by a circulating fluidized bed. Energy & Fuels, 2018, 32(10): 10956–10963.

[42] Zhu S., Zhu J., Lyu Q., Liu J., Ouyang Z., Pilot-scale study on NO emissions from coarse coal combustion preheated by circulating fluidized bed. Fuel, 2020, 280: 118563.

[43] Zhang H., Zhang Y., Zhu Z., Circulating fluidized bed gasification of low rank coal: influence of O_2/C molar ratio on gasification performance and sulphur transformation. Journal of Thermal Science, 2016, 25(4): 363–371.

[44] Man C., Zhu J., Ouyang Z., Experimental study on combustion characteristics of pulverized coal preheated in a circulating fluidized bed. Fuel Processing Technology, 2018, 172: 72–78.

[45] Leppalahti J., Kurkela E., Behaviour of nitrogen compounds and tars in fluidized bed air gasification of peat. Fuel, 1991, 70(4): 491–497.

[46] Xu W., Kumagai M., Nitrogen evolution during rapid hydropyrolysis of coal. Fuel, 2002, 81(18): 2325–2334.